FACULTY OF SCIENCE
UNIVERSITY OF COPENHAGEN

Eddy fluxes in the Norwegian Current

Johanne Kristine Bork Øelund

Master Thesis

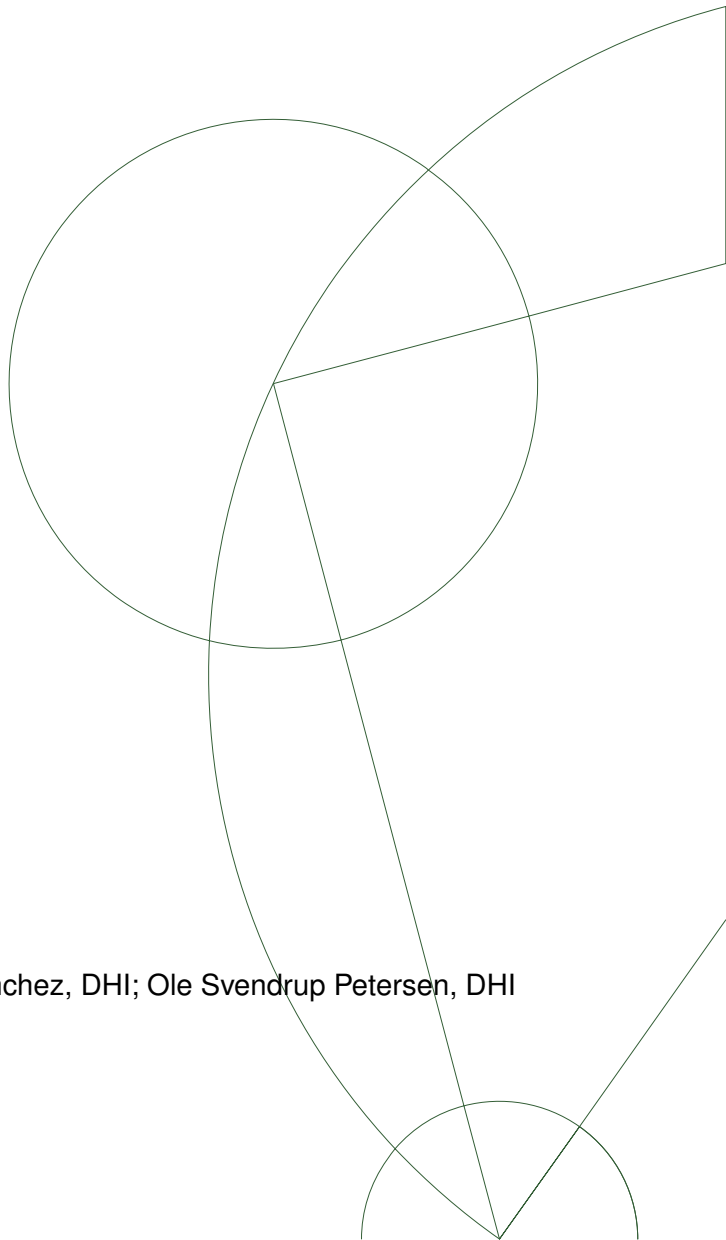

Supervisor: Markus Jochum, NBI; Rodolfo Baloños Sanchez, DHI; Ole Svendrup Petersen, DHI

June 30, 2016

"*Big whirls have little whirls*
That feed of their velocity
And little whirls have lesser whirls
And so on to viscosity"

L. F. Richardson

Abstract

The circulation of the Norwegian Sea has a great influence on the relatively mild climate in Norway by transporting warm Atlantic water towards the Arctic. The warm, saline water is transported by the Atlantic current to the Norwegian Sea where topography steers the current and creates eddy activity which elongates the Atlantic waters circulation time in the Norwegian Sea.

Using a MIKE powered by DHI model the Norwegian Atlantic Current is studied and analysed to find how well the current is represented.
The Norwegian Atlantic Current is known to bifurcate in the Norwegian Sea, but the MIKE model was only able to present the slope current, which is the eastern branch of the Norwegian Atlantic Current, and partially the Norwegian Coastal Current.

By combining the data from the current velocity, temperature and salinity an estimate of the heat transport through the Norwegian Sea is calculated.
The data shows a great seasonal variation in the magnitude of current velocity, transport and eddy activity.

Resumé

Cirkulationen i Norskehavet har en stor indflydelse på det relativte milde klima i Norge da den transporterer varmt Atlantisk havvand mod Arktis.
Det varme, saltholdige vand transporteres af den Atlantiske havstrøm til Norskehavet, hvor topografien styrer havstrømmen videre og skaber eddy aktivitet, som forlænger det Atlantiske vands cirkulations tid i Norskehavet.

Ved brug af en MIKE powered by DHI model er den Norske Atlantiske havstrøm blevet undersøgt og analyseret for at finde ud af, hvor godt havstrømmen er repræsenteret.
Den Norske Atlantiske havstrøm er kendt for at tvedele sig i Norskehavet, men MIKE-modellen var kun i stand til at præsentere havstrømmen over den kontinentale skråning ud fra Norges kyst, som er den østlige gren af den Norske Atlantiske Havstrøm, og delvist den norske kyststrøm.

Ved at kombinere data fra strømhastigheden, temperatur og saltindhold er et estimat af varme transporten gennem Norskehavet beregnet.
Dataen viser en stor sæsonbetonet variation af størrelsen af havstrømme, transport og eddy aktivitet.

Acknowledgements

First of all I would like to thank my supervisor Markus Jochum for guidance and letting me be part of Team Ocean. It has been interesting.
I am grateful for the advices and techical assistance I have recieved from Rodolfo Baloños Sanchez and Ole Svendrup Petersen, and to DHI and Statiol for letting me work with their data.
I am thankful for the grafical help from Christian Øelund.
Thanks to Signe Schilling, Tina Bay and Peter Martin Haandbæk for proofreading and being patient with me.

Finally a belated thank you to Vagner Jacobsen for a good advise many, many years ago.

Contents

List of Figures

List of Tables

List of Abbreviations

AW	**A**tlantic **W**ater
EKE	**E**ddy **K**inetic **E**nergy
LB	**L**ofoten **B**asin
NCC	**N**orwegian **C**oastal **C**urrent
NS	**N**orwegian **S**ea
NwAC	**N**orwegian **A**tlantic **C**urrent
NwAFC	**N**orwegian **A**tlantic **F**ront **C**urrent
NwASC	**N**orwegian **A**tlantic **S**lope **C**urrent
SSH	**S**ea **S**urface **H**eight

Physical Constants

Gravitational acceleration	$g = 9.806\,65\,\mathrm{m/s^2}$
Reference density of water	$\rho_0 = 1025\,\mathrm{kg/m^3}$
Rotation rate of the Earth	$\Omega = 7.2921 \times 10^{-5}\,\mathrm{s^{-1}}$
Prandtl number	$\sigma_T = 13.4$ for seawater at $0^{\circ}C$, 9.47 at $10^{\circ}C$
Specific heat	$c_p = 4217$ J/kg $^{\circ}K$

List of Symbols

d	still water depth	m
f	Coriolis parameter	s^{-1}
h	total water depth	m
p_a	atmospheric pressure	Pa
$s_{xx}, s_{xy}, s_{yx}, s_{yy}$	radiation stress tensor	kg/ms^2
t	time	s
v_t	vertical turbulent viscosity (eddy)	m^2/s
$\mathbf{u}$	current velocity	$m\,s^{-1}$
u, v, z	velocity components	$m\,s^{-1}$
u_s, v_s	discharge velocity	$m\,s^{-1}$
x, y, z	cartesian coordinates	
L	length	m
R_d	Rossby radius of deformation	m
S	magnitude of discharge	m^3/s
T	temperature	C
η	surface elevation	m
ρ	density of water	kg/m^3
ϕ	latitude	

Chapter 1

Introduction

The Norwegian Sea (NS) has been of interest to science since it has been shown that the movement of the currents has a great effect on the climate in the Arctic and the surrounding countries.

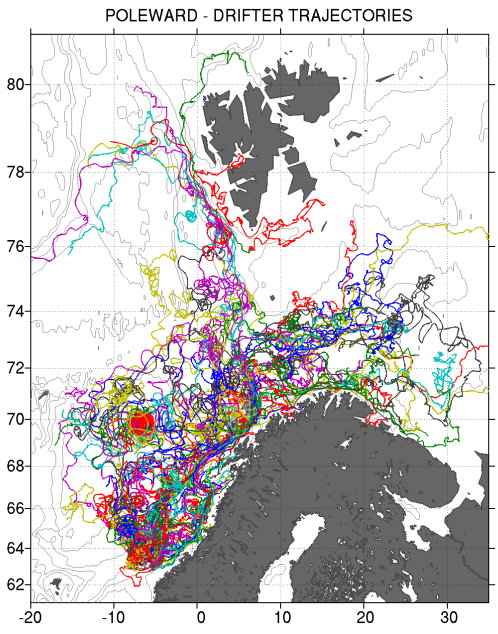

FIGURE 1.1: *The chaotic trajectery of drifter buoys (POLEWARD project).*

During the last decade an alarming climate change has been observed in the Arctic (Grotefendt et al., 1998). The temperature has risen, resulting in the melting of glaciers and sea-ice. These changes are presumed to be related to an increase of poleward transport of heat through the ocean, making it interesting to study the variation of the heat flux.

It is the chaotic movement in the Nordic sea that warms the area. If the current, with a supposed velocity of 1 $\mathrm{m\,s^{-1}}$ flowed steadily along the coast, it would travel from the south of Norway to Svalbard in only 60 days. This would resolve in considerably colder climate in Norway, seeing that less heat would be transferred to the atmosphere, compared to the actual turbulent flow of the ocean, where the current takes more than 500 days to flow past Norway, figure 1.1 (Amundsen and Lie, 2011).

The transport of warm water from the equator to the northern hemisphere is an important factor for the climate and biological production. Especially the fishing industry has a great interest in this seeing that the circulation influences the transport and spreading of fish eggs and nutrients in the water (Sætre and Ljøen, 1972).
From the perspective of global warming the temperature and amount of water being transported from the south into the Norwegian Sea and further towards the Arctic is of great importance.

Eddies influence on the climate comes from their effect on ocean circulation in regards to transport and mixing temperature and salt, and extracting potential energy from the mean current. Even though the eddy contribution to the meridional transport of water masses is small in many regions, it can not be ignored on the global scale.The NS has been found to have high mesoscale eddy activity especially in the region between the large currents in the area.

This thesis aims to elucidate how well an oceanic model represent the various movements in the NS, by looking in to and compare data of velocity, salinity and temperature with other models and in-situ measurements.

1.1 Historic surveys

During the last century there has been many expeditions exploring the NS in an attempt to understand and map out the current movement, salinity and temperature distribution, with the aid of vessels, drifters, buoys and later on satellites.

The first time the Atlantic currents movement in the Norwegian sea was mentioned in literature was in 1578:

"with a great currante from oute of south-west which carryed us (by our reconition) one point to the north-eastwardes of our said course, which currant seemed to us to continue itselfe towards Norway and other north-east partes of the world"

Martin Frobisher (3rd voyage).

but even the old Norsemen realised the existence of a great current moving the ice around the ocean.

The earliest "modern" scientific survey was carried out in 1900-1904 by Björn Helland-Hansen and Fridtjof Nansen.
During the four years of expeditions Helland-Hansen and Nansen (1909) carried out ten expeditions in the period between February and November, most of them in the summer period. They did surface current observations every hour, but since the procedure for deep measurements was troublesome there was only made a few measurement from deeper ocean. All their current measurements was made in the summer and there is no recordings of current velocities in other seasons.

FIGURE 1.2: *Historic observations of the circulation i NS (Helland-Hansen and Nansen, 1909).*

Their main focus was to show the vertical distribution of salinity and temperature. By looking at this distribution they found great irregularities, sometimes in the form of horizontal waves and entitled these ocean features puzzling waves, now known as eddies. They considered the possibility that these were caused by the configuration of the coast and the bathymetry. They also discovered evidence of a great puzzling wave at Lofoten indicated vortices in the Atlantic current, later this was found to be a quasi permanent vortex residing in the Lofoten Basin (LB).

Their prediction regarding the movement of the currents is in agreement with modern day surveys, figure 1.2.

1.2 The Region

1.2.1 Circulation in the Norwegian Sea

The Norwegian Sea is dominated by the inflow of Atlantic Water (AW) and outflow of the Norwegian currents. The AW enters the NS as the remaining part of the Gulf stream, but also the current coming from the Baltic Sea effects the movement in the Norwegian sea.
Poulain, Warn-Varnes, and Niiler (1996) found by deployed drifters that the AW flowing into the NS are mostly topographical steered.

Studies have shown that there is a large exchange of water between the different currents in the NS, which can make it hard to distinguish one currents from another, especially in areas where they move closely together(Orvik, Skagseth, and Mork, 2001).

1.2.2 Norwegian Atlantic Current

The Norwegian Atlantic Current (NwAC) is the northern extension of the North Atlantic Current (NAC) coming from the Gulf Stream, where it transports warm saline AW towards the Barents Sea and Arctic Ocean.
The NwAC flows into the Norwegian Sea through the Faroe-Shetland channel and at the Faroe-Iceland ridge with a temperature of $6 - 10°C$. It follows the topographical contours of the continental slope towards Norway before it bifurcates into two branches, the NwAFC and NwASC which are strongly steered by topography.

There has been observed such a significant exchange of water between the two branches, making it difficult to distinguish them, that it have been discussed if they could in fact be defined as two independent currents (Poulain, Warn-Varnes, and Niiler, 1996; Orvik and Niiler, 2002).

When the AW reaches the Fram strait, the water temperature will be well below $5°C$. At this point the cold current dives beneath the cold Arctic waters and flows back to the Atlantic at $4000 - 5000$ m depth, where it can be submerged in centuries. (Amundsen and Lie, 2011; Orvik, 2004)

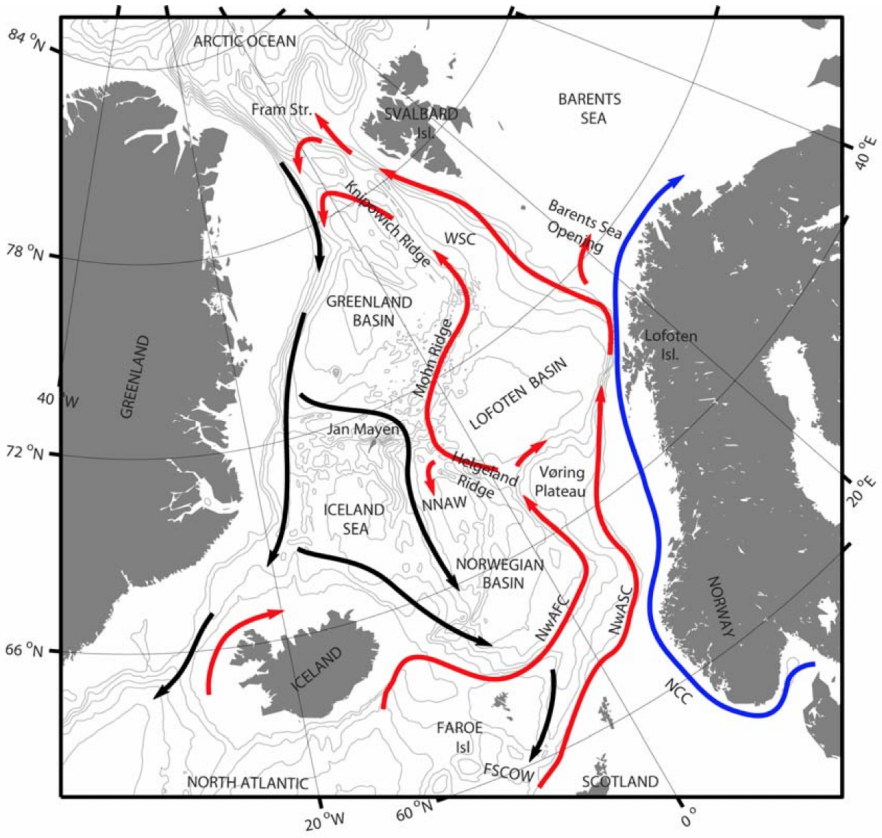

FIGURE 1.3: *The major current pathways near-surface in The Norwegian Sea (Raj, 2013).*

The NwAC maintain the two branch structure throughout the NS confining the AW to a wide wedge.
Orvik and Niiler (2002) found through their study using Lagrangian drifters at 15 m depth, that the major currents could be identified with average current speed above 30 cm s^{-1}.

Norwegian Atlantic frontal Current

The Norwegian Atlantic Front Current (NwAFC) is the western branch of the NwAC as seen in figure 1.3.
It enters NS between Iceland and the Faroe islands, and continues eastward towards Norway. It passes through the Svinøy section, in the south of Norway, where it follows the topographic slope of the Vøring Plateau travelling north-west towards Jan Mayen. Hereafter the current continues a path north-east along the Mohn's Ridge and thereafter towards Fram Strait.

The NwAFC is found to be an unstable frontal jet at around 400 m depth and approximately 30-50 km wide, it is associated with a temperature front (Orvik, Skagseth, and Mork, 2001; Orvik and Niiler, 2002).

Norwegian Atlantic Slope Current

The Norwegian Atlantic Slope Current (NwASC) is the easterly branch of the NwAC as seen in figure 1.3.
It enters the NS between the Faroe island and Scotland, and travels towards Norway just south of the NwAFC following the continental slope along Norway closely. A small branch of the NwASC rounds the North Sea, mixing with the water from the Baltic Sea and the North Sea before it continues northward to the Svinøy section.
At the northern part of Norway a part of the current continues to follow the shoreline towards the Barents Sea, but the majority of the current continues north towards Fram Strait(Ljøen and Nakken, 1969).

The NwASC travels nearly 3500 km along the shelf edge and is wedged formed with a width of 30-50 km, and the unstable structure of the current acts as a trigger for eddy shedding and recirculation (Orvik and Niiler, 2002; Orvik, Skagseth, and Mork, 2001)

1.2.3 The Norwegian Coastal Current

The Norwegian Coastal Current (NCC) is an important part of the NS circulation system. It consists of brackish water from the Baltic Sea and North Sea, fresh water from river discharge and the Norwegian fjords mixed with Atlantic water. This results in a strong, low saline coastal current that runs in the upper $50 - 100m$, closely following the bathymetry of the Norwegian continental shelf northward to the Barents sea and the Arctic. The NCC is primarily driven by density gradient, but also by gradient in sea-level (Sætre and Ljøen, 1972; Oey and Chen, 1992).
(Pedersen et al., 2005) described the NCC as a baroclinic unstable current that forms cyclonic and anticyclonic eddies along the zone between the fresher water of NCC and the saline water of NwASC.

The NCC has a western boundary formed by the inflowing AW which is warmer and more saline. The average temperature of the NCC is in the range of $2 - 5°C$ and the salinity is less than 34.8 psu, for the AW the average temperature is above

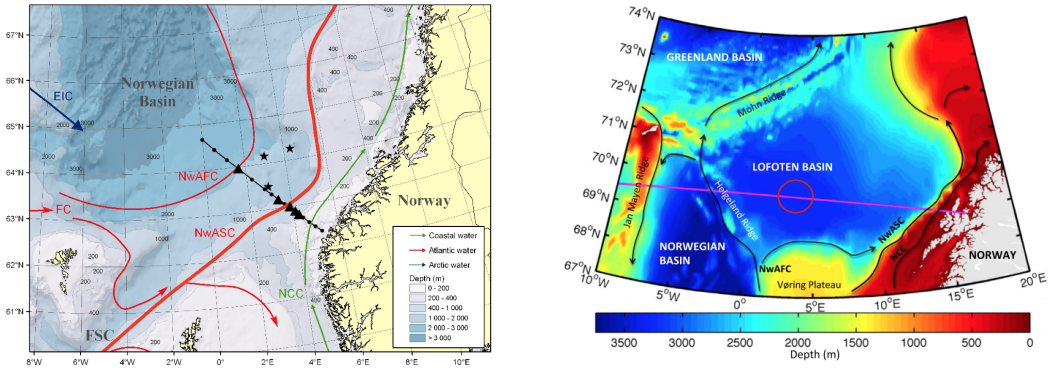

(A) *The Svinøy section (Mork and Skagseth, 2010)* (B) *The Lofoten area (Volkov, Kubryakov, and Lumpkin, 2015)*

FIGURE 1.4: *Key areas in the Norwegian Sea*

$6°C$ and the salinity above 35 psu.
Due to the comprehensive mixing with the AW, both vertically and horizontally, the salinity gradually increases as the current moves further north while the temperature decreases due to the heat loss to the surroundings (Sætre and Ljøen, 1972; Ikeda et al., 1988).

Mork (1981) and Oey and Chen (1992) found that north-westerly wind increases the transport for NCC at the south of Norway, which is in contrast to the Ekman's theory of wind driven coastal circulation, but by taking the whole NS into account this can be explained by the structure of the bathymetry which has shown to raise a strong cyclonic circulation for this wind-direction. The variable movement of Baltic origin water in the NCC is often a result of variation in the wind-stress over the North Sea, this effect propagates along the shore of Norway and contributes to the dynamic forcing further north.

1.3 Key area

The NS is located between the North Sea and the Greenland Sea. It is separated in the southwest from the Atlantic Ocean by a ridge running between Iceland and the Faroe Islands. To the North, the Mohn's Ridge separates it from the Greenland Sea, figure 1.3.
The NS has been under thorough survey for the last century, where the focus especially has been on two sections of the ocean as shown in figure 1.4.

1.3.1 Svinøy section

Since 1995 an ongoing survey have monitored the water at the Svinøy section. Up to 17 hydrographic stations, covering the 3 currents described above at various depths.
This area is of especially interests because all the currents are passing through a topographical confined area where the variation in velocity and the different steering for the currents can be monitored easily.

The Svinøy section goes from $62°N$ crossing the shore of Norway to $64°40'N$ at the prime meridian, figure 1.4a.

1.3.2 Lofoten Basin

The Lofoten Basin (LB) is the major heat-reservoir in the NS with a volume of approximately $5 \cdot 10^5\ km^2$. The water in LB consist of warm saline AW occupying the upper 600-700 m, transported there by mesoscale eddies since there is no mean flow into the basin.
The region is found to have a high mesoscale activity, it is therefore an important area regarding the climate in the northern ocean, since eddies flux heat from the continental slope into the interior of LB which balances the heat loss from the basin to the atmosphere.
The LB is enclosed by the NwAFC to the left and NwASC to the right due to the well defined topographic depression.
LB is characterized by a strong, mostly cyclonic eddy field, originally created by the instability of NwASC, and a quasi-permanent anti-cyclonic vortex in the center, which makes the AW reside in the basin for a long period. The eddies are thought to be hold stable in the basin by the topography defining the LB. Eddies migrate into the center of the basin, maintaining the quasi-permanent vortex (Orvik, 2004; Poulain, Warn-Varnes, and Niiler, 1996; Köhl, 2007; Volkov, Kubryakov, and Lumpkin, 2015).

The Lofoten section goes from $72°N$ to $68°N$ and $0°$ to $15°E$ with the center of the LB marked with the red circle in figure 1.4b.

The water temperature drops from ca. $5 - 10°C$ near Svinøy in the south to $3 - 6°C$ near LB in the north.

1.3.3 Water composition

The different currents brings water with different composition. The NS consists roughly of 3 different water types: Atlantic water, coastal water and deep water. The deep water can then again be divided into Norwegian Sea deep water, which is the densest water in the NS, and Greenland Sea deep water, which is the coldest mostly around $-1.1°C$, but for an easy overview the deep sea water is combined, table 1.1.
By distinguishing between the different values of salinity and temperature the origin of the current can be established (Mysak and Schott, 1977; Blindheim, 1990; Orvik, Skagseth, and Mork, 2001).

TABLE 1.1: *Description of water composition.*

Water	Temperature $[°C]$	Salinity [psu]
Atlantic water	> 5	> 35
Coastal water	< 5	< 35
Deep water	< -0.5	34.92

1.4 Eddies in the ocean

When looking at the oceans from space, large distinct current like the Gulf Stream are clearly visual, but the water inside those large gyres are also moving, sometimes even as fast as the major current, but these are unsteady.
Mesoscaled eddies was only first thoroughly examined and named in the 1960's, but the circular motions of eddies was observed early 1900 as mentioned.
Eddies can vary in size from a few centimetres up to 100 km i diameter, the smallest scale eddies can last for only seconds while large scaled can live for many month with a measured velocity between $0.04 - 0.4\ \mathrm{m\,s^{-1}}$.
With the length and timescale lying in this range, the Rossby number is low $R_0 \sim 0.04$ and thereby the eddy velocity is geostropic. A small Rossby number signifies that a system is strongly effected by Coriolis force where a large Rossby number signifies a system where initial and centrifugal forces are dominant (Knauss, 1997).

Eddies occurs when a current nips off a section and creates a circular current, with high energy currents generating mesoscale meanders, which grows and eventually detach from the main current. In general the Coriolis effect causes the

warm and saline eddies to rotate cyclonic, and the cold, fresh eddies to rotate anti-cyclonic in the northern hemisphere at eastern boundaries. The larger eddies can take a few days to rotate while drifting slowly (Pedersen et al., 2005), figure 1.5. Oceanic eddies usually consist of a water mass deviating in temperature, salinity, heat etc. from the water outside the eddy.

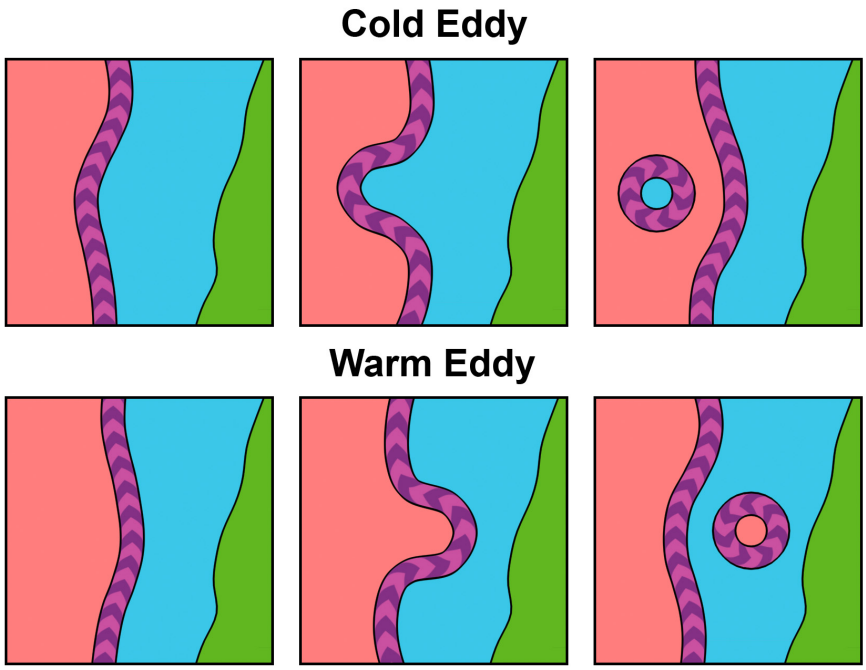

FIGURE 1.5: *Eddy creation by movement of current.*

One of the most important mechanisms in eddy development is the baroclinic instability. The swirls of the eddy can bring colder and more nutrient rich deeper water to the surface.

Eddies play a major role in the structure of the oceans by transporting and mixing energy and chemicals throughout the basins sustaining a great deal of oceanic life. Eddies can travel over long distances for months before dissolving. They are relatively small swirls of water that has broken off main currents and travel independent of these.

Once the strong main current no longer is restricted by the influence of land, it becomes unstable and begins to meander. If the current becomes to bend, this section can pinch off, separating it from the current.

Eddies can also be formed in mid ocean. This formation is a result of an unstable process where large scale mean flows are breaking down to smaller scale features. The eddies carry water and heat across large distances and assist with the large

scale mixing of the ocean, distributing nutrient, salt and other chemicals throughout.

The strong currents and eddies can damage oil-platforms and erode the land. Mesoscaled eddies are in the range of $10 \rightarrow 500$ km in diameter and can persist for periods of up to months holding large amount of eddy kinetic energy.
The eddies between the NCC and NwASC are found to be in the range of $50 - 100$ km in diameter, with the cyclonic eddies tending to be a somewhat smaller in size and having less velocity than anticyclonic eddies (Mork, 1981; Hansen, Kvaleberg, and Samuelsen, 2010; Volkov, Kubryakov, and Lumpkin, 2015) .

Eddies are vital for transport and mixing in the ocean. Larger eddies generate smaller eddies and so on.
In order to observe eddies different techniques are used. Surface eddies can be viewed by satellite images, surveying the SST as in figure 1.6 where formation of cyclonic eddies (denoted CE) and anticyclonic eddies (denoted AE) are shown.
Since electromagnetic beams from satellites are absorbed by the ocean, research ships and autonomous instruments are used to achieve information on the deeper structure of the eddies in the oceans.
The disadvantage of this method is that they can only gather samples from a small section of the many eddies at one time so generally computer- and theoretical models are used.

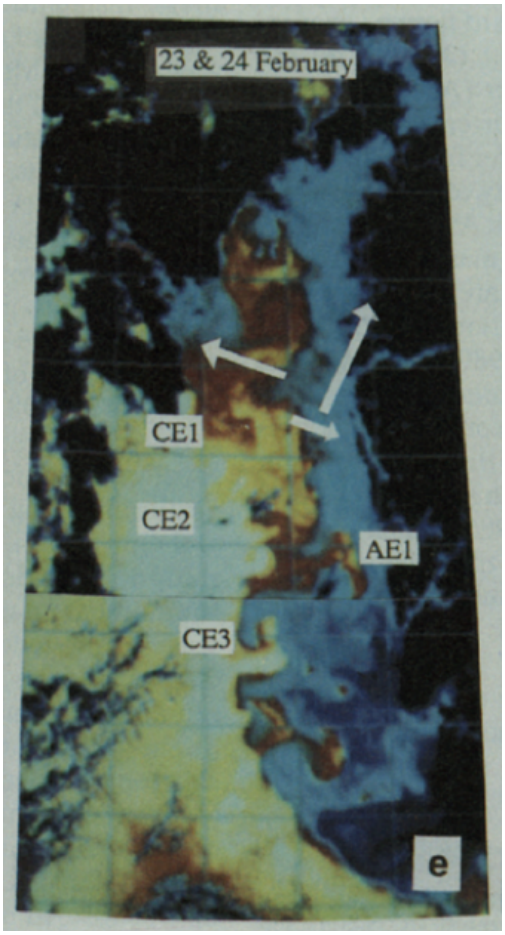

FIGURE 1.6: *IR image of the south-west coast of Norway (Johannessen et al., 1989).*

Computer models divides the ocean into a spacial grid and solves the physical equation for each cell. The grid size has to be

small enough to view the mesoscale eddies, but small grids means more equations to be solved which will require a larger amount of computer processing power. So in order to be able to work easily with the data a compromise most be made regarding the size making it small enough to see the larger eddies, eliminating the small eddy data.

The most commonly used methods in gathering information and data for eddy surveys are: satellite altimetry (measuring SSH), radar, acoustical and current measurements.

Some surveys indicates that the NwASC transports warm water to the LB via eddies (Andersson et al., 2011).
By satellite images the NCC has been found to break up into eddies in the order of $50km$ due to the currents instability (James, 1991). Radar satellite images of the Norwegian coastal water have shown that surface eddies with a diameter of approximately 10 km are most common (Johannessen et al., 2005).
Mork (1981) found that meanders and eddies are created by the interaction between the variation of the wind and the rough, irregular bathymetry in the Norwegian area.
Ikeda et al. (1988) studied the eddies in the region south-west of Norway and found that baroclinic instability was one of the main reasons to forming meanders at the current fronts and the importance of the topography in the formation of eddies, which was also noticed by (Johannessen et al., 1989) in a study west of Norway, which also included topographic steering and vortex stretching as reasons for eddy formation.

The eddies found at LB are primarily formed by the instability of the NwASC and are thought to have a significant part in the heat exchange and dense water formation (Volkov, Kubryakov, and Lumpkin, 2015).

1.4.1 Eddy heat flux

Eddy heat fluxes are thought to have an important cooling effect on the NwASC and NwAFC as they move though the NS.

Orvik and Skagseth (2005) observed an extra ordinary warming of the AW flowing into the NS towards the Arctic during the last decade, a downward 10 year trend in velocity of 3.9 $\mathrm{cm\,s^{-1}}$ and a $1°C$ increase in temperature. The effect

on the climate by this could be found by studying the variation of the heat flux in NwASC seasonally and annually.

1.4.2 Eddy kinetic energy

Eddy Kinetic Energy (EKE) is the energy of the ocean associated with the turbulent flow of the currents. It derives its energy from the mean circulation, resulting in greater EKE where the mean circulation is strongest.

The oceans kinetic energy can be divided into two parts, one representing the time mean of the flow and one representing the eddy.
Through buoyant drifter observation it is known that the EKE is many times greater than the kinetic energy of the mean flow, meaning that the ocean circulations are dynamic and turbulent (Knauss, 1997).

1.5 Objectives

The main objective of this study is to validate the hydrodynamic model by MIKE 3 in the Norwegian Sea by exploring the following:

- To examine the variability of the circulation of the Norwegian Sea.
- To identify the different flows.
- To study the vertical structure of the current, salinity and temperature.
- To identify the eddy activity in the Norwegian Sea by looking at eddy kinetic energy and eddy heat flux.
- To validate the models representation of the various features in the Norwegian Sea.

Chapter 2

Model description and methods

The dataset used in this thesis is made by the program MIKE powered by DHI and includes the effect of tides, meteorological forcing, oceanographical forcing and general oceanographic circulations. The model is based on two older MIKE models, one covering the North Sea and one covering the Barents Sea.
The model was set up using bathymetry, computational mesh and forcing data, and thoroughly calibrated using the two previous models through different steps:

- Tide-only calibration
- Total water level calibration (tidal, meteorological and oceanographical)
- Salinity and temperature calibration
- Total current calibration

2.1 Mike program

For the Norwegian Ocean a model by MIKE3/MIKE21 by DHI was used. The model gives data for current, direction, salinity and temperature. The model runs over a period of 2 years from 1/12 -2012 to 31/12-2012, with timesteps of one hour. The dataset was initially created for oil and gas drilling in the Norwegian waters.

The MIKE model was developed to solve complex functions in oceanography, coastal- and estuarine environments.

2.1.1 The model

The model consists of an horizontally irregular triangular mesh, with a resolution varying from approximately 13 km in the off-shore regions 2.1a, 8 km closer to the shore and 3 km near shore 2.1b.

The mesh used in the model for the Norwegian Sea is composed of 50096 nodes and 88952 elements, with a resolution between $0.3 - 0.003°$.

Vertically the model consists of 33 layers. The 13 layers closest to the surface are depth varying sigma layers and the remaining 20 layers are z-layer with a constant depth as seen in figure 2.2. By using sigma layering the model will have a higher accuracy and a smoother representation of the bathymetry and a consistent resolution near the shore and ocean bed. The disadvantages of using sigma layering is a greater possibility of significant errors in the horizontal pressure gradient, advection and mixing near steep slopes which will result in unrealistic flows. The calculations of horizontal pressure gradient, advection and mixing are more simple using z-layering, but this is proven inaccurate, when it comes to representation of the bathymetry. Since the z-layers gives a squared slope representation, this can give an unrealistic flow near the ocean bottom and slopes.

2.1.2 Initial and lateral boundary conditions

The boundaries along the coastline are closed, setting all normal fluxes for all variables to 0. This results in no shear of flow parallel to the coast and thereby no frictional stress imposed on the flow leading to full-slip along land boundaries for the momentum equation. The open boundaries are forced by elevation, current velocities, salinity and temperature.
The initial conditions for the open boundary for salinity and temperature used in the model were provided by MyOcean, and the initial conditions for the open boundary for surface elevation and the various components for the current were a combination of MyOcean[1] and A Tidal[2] results. Since MyOcean did not account for ties additional tidal height and current were added using the DTU10 global tidal model[3].

The model has been calibrated in regard to wind, tidal current, water level, surface temperature, surface salinity, surface current and current throughout the water column in locations close to the shore along the coastline of Norway (Rugbjerg, 2014; Cheng and Andersen, 2010).

[1] International association collecting satellite and in-situ measurements for ocean monitoring and forecasting.
[2] based on TOPEX/POSEIDON satellite data.
[3] global ocean tide model using 17 years of measurements from TOPEX/POSEIDON, Jason-1 and Jason-2 satellite altimetry.

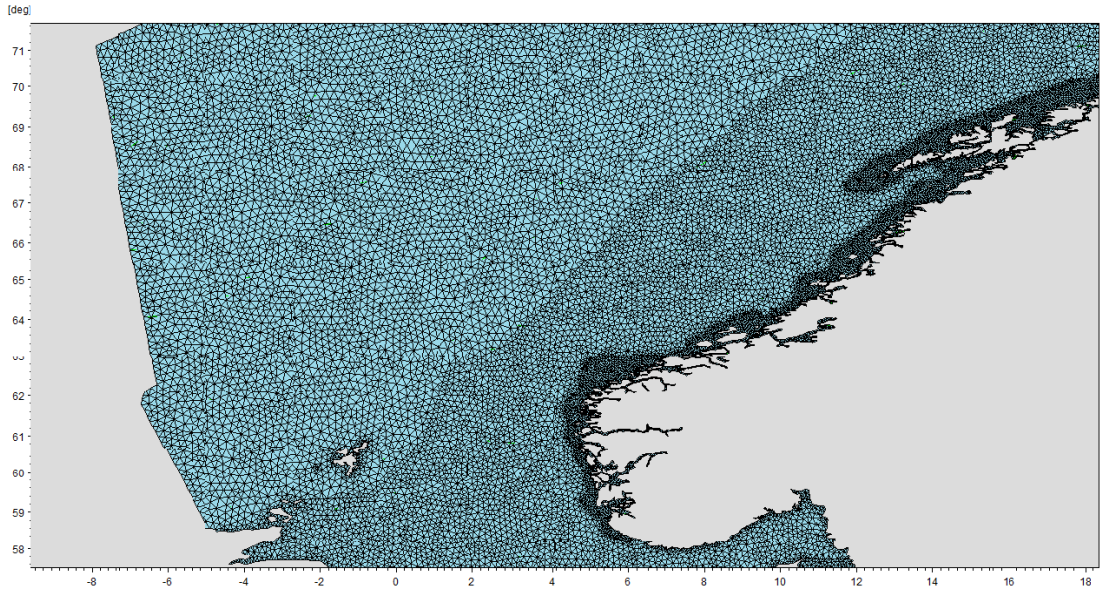

(A) *Grid offshore*

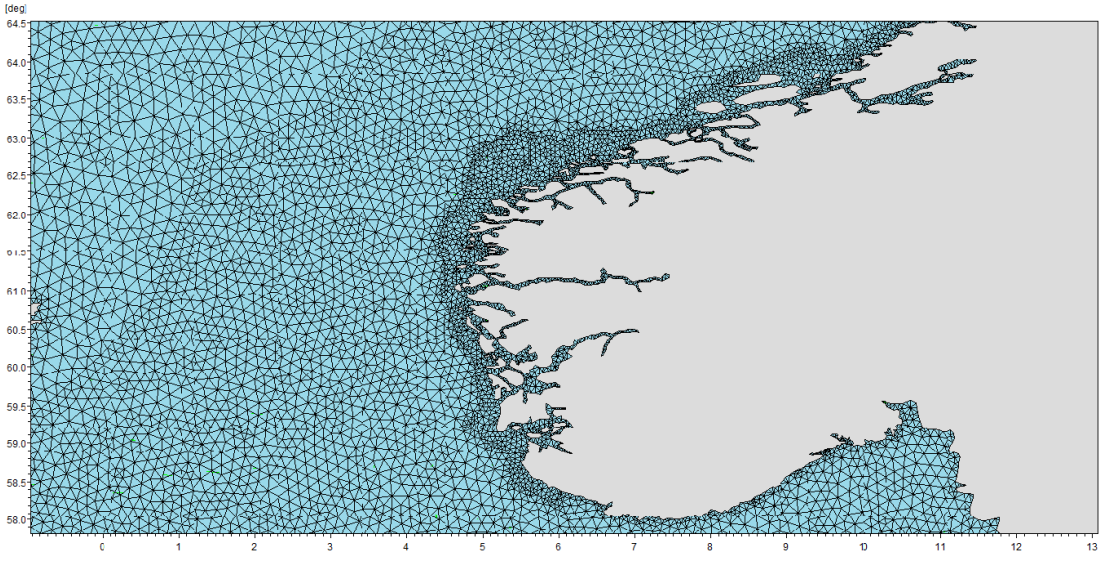

(B) *Grid near shore.*

FIGURE 2.1: *The irregular triangular grid of the MIKE model.*

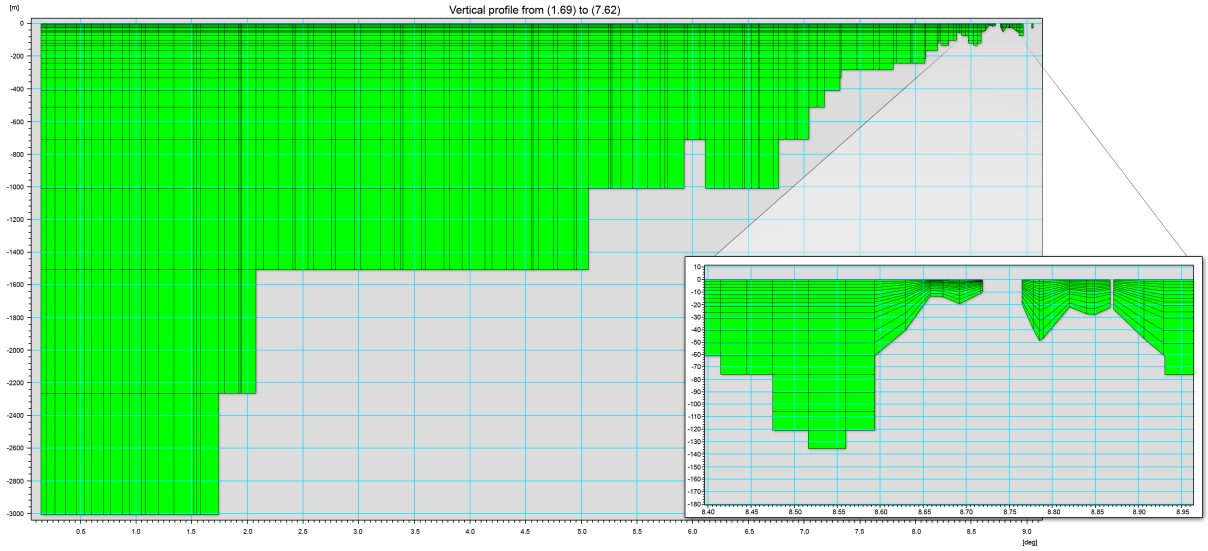

FIGURE 2.2: *Vertical view of the different layers in the model.*

2.2 Governing equation

MIKE3 is based on a numerical solution of the three-dimensional incompressible Reynolds averaged Navier-Stokes equation with the assumption of Boussinesq and hydrostatic pressure (DHI, 2014).

The model consists of 5 general equations:

- Continuity equation
- Momentum equation
- Temperature transport equation
- Salinity transport equation
- Density equation

The continuity equation is written as:

$$\frac{\partial u}{\partial x} + \frac{\partial v}{\partial y} + \frac{\partial w}{\partial z} = S \tag{2.1}$$

The two horizontal momentum equations for the x- and y-component are written as:

$$\underbrace{\frac{\partial u}{\partial t}}_{1} + \underbrace{\frac{\partial u^2}{\partial x} + \frac{\partial vu}{\partial y} + \frac{\partial wu}{\partial z}}_{2} = \underbrace{fv}_{3} - \underbrace{g\frac{\partial \eta}{\partial x}}_{4} - \underbrace{\frac{1}{\rho_0}\frac{\partial p_a}{\partial x}}_{5} - \underbrace{\frac{g}{\rho_0}\int_z \eta \frac{\partial \rho}{\partial x} dz}_{6} - \underbrace{\frac{1}{\rho_0 h}\left(\frac{\partial s_{xx}}{\partial x} + \frac{\partial s_{xy}}{\partial y}\right)}_{7} + \underbrace{F_u + \frac{\partial}{\partial z}\left(v_t \frac{\partial u}{\partial z}\right)}_{8} + \underbrace{u_s S}_{9} \quad (2.2)$$

$$\underbrace{\frac{\partial v}{\partial t}}_{1} + \underbrace{\frac{\partial v^2}{\partial y} + \frac{\partial uv}{\partial x} + \frac{\partial wv}{\partial z}}_{2} = \underbrace{-fu}_{3} - \underbrace{g\frac{\partial \eta}{\partial y}}_{4} - \underbrace{\frac{1}{\rho_0}\frac{\partial p_a}{\partial y}}_{5} - \underbrace{\frac{g}{\rho_0}\int_z \eta \frac{\partial \rho}{\partial y} dz}_{6} - \underbrace{\frac{1}{\rho_0 h}\left(\frac{\partial s_{yx}}{\partial x} + \frac{\partial s_{yy}}{\partial y}\right)}_{7} + \underbrace{F_v + \frac{\partial}{\partial z}\left(v_t \frac{\partial v}{\partial z}\right)}_{8} + \underbrace{v_s S}_{9} \quad (2.3)$$

with $h = \eta + d$ and $f = 2\Omega \sin \phi$.

The numbers refer to the different terms:

1. Acceleration
2. Advection
3. Coriolis force
4. Pressure buoyancy force
5. Atmospheric pressure
6. Pressure gradient
7. Radiational stress
8. Eddy viscosity, horizontally and vertically
9. Discharge

The horizontal stress terms F_u and F_v are described through a simplified gradient-stress relation:

$$F_u = \frac{\partial}{\partial x}\left(2A\frac{\partial u}{\partial x}\right) + \frac{\partial}{\partial y}\left(A\left(\frac{\partial u}{\partial y} + \frac{\partial v}{\partial x}\right)\right) \quad (2.4)$$

$$F_v = \frac{\partial}{\partial y}\left(2A\frac{\partial v}{\partial y}\right) + \frac{\partial}{\partial x}\left(A\left(\frac{\partial u}{\partial y} + \frac{\partial v}{\partial x}\right)\right) \tag{2.5}$$

where A is the horizontal eddy viscosity.

The transport of temperature and salinity follow the general transport-diffusion equation:

$$\frac{\partial T}{\partial t} + \frac{\partial uT}{\partial x} + \frac{\partial vT}{\partial y} + \frac{\partial wT}{\partial z} = F_T + \frac{\partial}{\partial z}\left(D_v\frac{\partial T}{\partial z}\right) + \widehat{H} + T_s S \tag{2.6}$$

$$\frac{\partial s}{\partial t} + \frac{\partial us}{\partial x} + \frac{\partial vs}{\partial y} + \frac{\partial ws}{\partial z} = F_s + \frac{\partial}{\partial z}\left(D_v\frac{\partial s}{\partial z}\right) + s_s S \tag{2.7}$$

F_T and F_s are the horizontal diffusion terms for temperature and salinity respectively defined by $(F_T, F_s) = \left[\frac{\partial}{\partial x}\left(D_h\frac{\partial}{\partial x}\right) + \frac{\partial}{\partial y}\left(D_h\frac{\partial}{\partial y}\right)\right](T, s)$, where D_h is the horizontal diffusion coefficient and D_v the vertical, which can be related to the eddy viscosity by $D_h = \frac{A}{\sigma_T}$ and $D_v = \frac{v_t}{\sigma_T}$. $\widehat{H}$ is the source term due to heat exchange.

The fluid is assumed incompressible, making the density depended of temperature and salinity and independent of the pressure with the equation of state:

$$\rho = \rho\,(T, s) \tag{2.8}$$

The density is calculated in accordance to the UNESCO (1981) equation.

2.2.1 Boundary conditions

The boundary conditions for u, v and w at the surface $z = \eta$ and the bottom $z = -d$ are:
For $z = \eta$:

$$\frac{\partial \eta}{\partial t} + u\frac{\partial \eta}{\partial x} + v\frac{\partial \eta}{\partial y} - w = 0, \qquad \left(\frac{\partial u}{\partial z}, \frac{\partial v}{\partial z}\right) = \frac{1}{\rho_0 v_t}\left(\tau_{sx}, \tau_{sy}\right) \tag{2.9}$$

where (τ_{sx}, τ_{sy}) is the x and y components of the surface wind.

For $z = -d$:

$$u\frac{\partial d}{\partial x} + v\frac{\partial d}{\partial y} + w = 0, \qquad \left(\frac{\partial u}{\partial z}, \frac{\partial v}{\partial z}\right) = \frac{1}{\rho_0 v_t}\left(\tau_{bx}, \tau_{by}\right) \tag{2.10}$$

where (τ_{bx}, τ_{by}) is the x and y components of the bottom friction.

The boundary conditions for temperature and salinity at the surface and bottom are:
For $z = \eta$:

$$D_h \frac{\partial T}{\partial z} = \frac{Q_n}{\rho_0 c_p} + T_p \widehat{P} - T_e \widehat{E} \tag{2.11}$$

$$\frac{\partial s}{\partial z} = 0 \tag{2.12}$$

For $z = -d$:

$$\frac{\partial T}{\partial z} = 0 \tag{2.13}$$

$$\frac{\partial s}{\partial z} = 0 \tag{2.14}$$

$\widehat{P}$ is precipitation rate and $\widehat{E}$ is evaporation rate.

2.2.2 Eddy viscosity

In the $k - \varepsilon$ model the vertical eddy viscosity can be derived from the turbulence parameters:

$$v_t = c_\mu \frac{k^2}{\varepsilon} \tag{2.15}$$

where k is the turbulent kinetic energy (TKE), ε is the dissipation of TKE and c_μ is an empirical constant. k and ε is found from the transport equations:

$$\frac{\partial k}{\partial t} + \frac{\partial uk}{\partial x} + \frac{\partial vk}{\partial y} + \frac{\partial wk}{\partial z} = F_k + \frac{\partial}{\partial z}\left(\frac{v_t}{\sigma_k}\frac{\partial k}{\partial z}\right) + P + B - \varepsilon \tag{2.16}$$

$$\frac{\partial \varepsilon}{\partial t} + \frac{\partial u\varepsilon}{\partial x} + \frac{\partial v\varepsilon}{\partial y} + \frac{\partial w\varepsilon}{\partial z} = F_\varepsilon + \frac{\partial}{\partial z}\left(\frac{v_t}{\sigma_\varepsilon}\frac{\partial \varepsilon}{\partial z}\right) + \frac{\varepsilon}{k}\left(c_{1\varepsilon}P + c_{3\varepsilon}B - c_{2\varepsilon}\varepsilon\right) \tag{2.17}$$

P is the shear production and B is the buoyancy production.

The horizontal eddy viscosity can be calculated using the Smagorinsky-Lilly model

$$A = c_s^2 l^2 \sqrt{2 S_{ij} S_{ij}} \tag{2.18}$$

where c_s is a constant, l is the characteristic length and the deformation rate S_{ij} is given by eq 2.19 where $(i, j = 1, 2)$

$$S_{ij} = \frac{1}{2}\frac{\partial u_i}{\partial x_j} + \frac{\partial u_j}{\partial x_i}) \quad (2.19)$$

2.3 Model validation

The MIKE model for the Norwegian Sea has been validated by DHI (Rugbjerg, 2014) using available in-situ- and satellite measurements[4] for the different types of variables:

- Wind, 2 stations, data and wind speed measurements compares well, with a small $5 - 6\%$ overestimate.
- Tidal, 21 stations, data and predicted tide compares well.
- Water level, 5 stations, data and measured water levels compares well except for one station lying in the archipelago which is not accounted for in the model.
- Surface current - covering the average of the top 30 m, satellite data, the circular pattern of the Norwegian current is fairly recognizable in the northern part of the model.
- Current in water column, measured by three Statiol oil-rigs. Compared for three depth: top ($21 - 24$ m below surface), mid and near sea-bed. A good fit between measured and modelled current was hard to obtain. This can be caused by the single point measurements, where eddies can cause the current speed and direction to vary within a small timescale compared to the models data.
- Sea Surface Temperature (SST), satellite data, there is a good resemblance near shore, but off shore the model has a tendency to show a cooler SST than the satellite data shows. This could be caused by false initial temperature at the open boundaries or to much mixing in the model for large depth.
- Salinity, satellite data, the model data shows a very similar picture compared to the measurements.

[4] Noaa project and OSCAR(Ocean Surface Current Analyses - Real time

2.4 MIKE to Matlab

DHI provides a Matlab program to read the dfsu-files, but with the layers being both sigma and z-layers, the program could not recognize all the layers and only used the top layers.

In order to get around this, a small data extraction program was used to extract the data at selected depths, table 2.1 and 2.2.

TABLE 2.1: *σ-layers.*

Layer No	1	2	3	4	5	6	7	8	9	10	11	12	13	14
Depth $[m]$	0	-1	-3	-6	-9	-12	-15	-18	-21	-25	-30	-40	-50	-60

TABLE 2.2: *z-layers.*

Layer No	15	16	17	18	19	20	21	22	23	24
Depth $[m]$	-75	-90	-105	-120	-135	-150	-165	-180	-195	-215
Layer No	25	26	27	28	29	30	31	32	33	34
Depth $[m]$	-245	-285	-335	-410	-510	-710	-1010	-1510	-2260	3010

The program can extract 6 variables:

1. u-velocity $[\mathrm{m\,s^{-1}}]$
2. direction [deg]
3. current speed $[\mathrm{m\,s^{-1}}]$
4. direction [rad]
5. temperature$[^{\circ}C]$
6. Salinity [psu]

The program provided a 2-dimensional data-set instead of the initial 3-dimensional.

2.5 The section of Lofoten and Svinøy.

The key areas, Svinøy and Lofoten, are used for examining the distribution of salinity and temperature through the various depths.

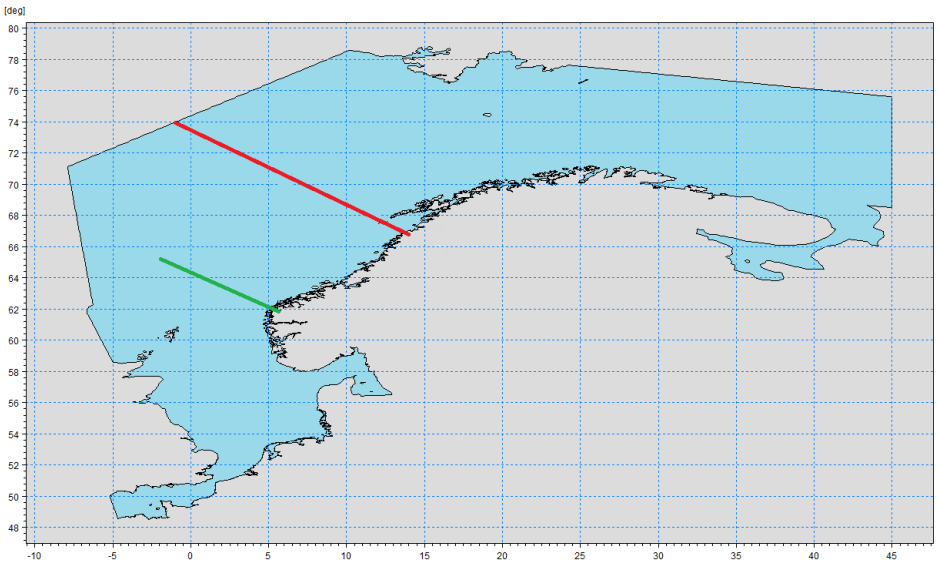

FIGURE 2.3: *Section cuts.*

The equation defining the Svinøy section is calculated be the positions of the mooring specified by (Skagseth and Orvik, 2002), green line in figure 2.3.

$$y = -0.44 \cdot x + 64.72 \tag{2.20}$$

with $x = -2 : 6$.

The equation of Lofoten is calculated so the line goes through the center of the LB and should include both NwASC and NwAFS, red line in figure 2.3.

$$y = -0.49 \cdot x + 73.51 \tag{2.21}$$

with $x = -1 : 14$.

2.6 Transport

The amount of warm, saline AW transported through the key section is calculated as the depth integrated velocity:

$$Tr = \int_A \mathbf{u} \cdot dA \tag{2.22}$$

Since AW has a high salinity, the transport has been calculated specific for velocity of water with salinity > 35 psu.

2.7 Rossby number

In order to know what forces dominates the rotation and movement, the Rossby number R_0 is used.

$$R_0 = \frac{\mathbf{u}}{f \cdot L} \tag{2.23}$$

For a system with a large Rossby number, the dominant forces are the inertial and centrifugal forces and the effect of the planetary rotation can be neglected. This occurs either if f is small (at low latitudes), L is small (small scale motion) or for large velocities. For a small Rossby number the system is in geostropic balance (geostropic eq).
(Oey and Chen, 1992) found that for $R_0 < 0.1$ eddies stay close to topographic features while for large R_0 eddies move away from the obstacle.

2.8 Eddy

There is an increasing interest in heat transport by mesoscale eddies in the ocean because it is thought to be an important term in the time mean ocean heat transport. The eddy heat transport occurs from velocity and temperature variabilities around their time-mean, but the fundamental dynamics of the eddy heat transport is still not adequately clear. Furthermore the time-mean eddy heat transport is one of the most poorly observed variabilities in the ocean.
In simulated ocean-models it is important to have the right resolution. If the resolution is to low, the simulated eddy kinetic energy will be to weak, while a higher resolution model can provide a more adequate picture of the eddy heat transports magnitude and general structure (Jayne and Marotzke, 2002).

2.8.1 Rossby radius of deformation

In order to see if a model has a sufficiently small grid size the Rossby radius of deformation R_d can be applied.

$$R_d = \frac{\sqrt{(g \cdot h)}}{f} \tag{2.24}$$

The size of ocean eddies varies with latitude. In low latitude regions, eddies are much larger than in high latitude regions R_d denotes the length scale at which rotational effects become as important as buoyancy or gravity wave effects in the evolution of the flow about some disturbance.

The general Rossby radius of deformation in the NS is ~ 10 km and the dominant eddy scale is ~ 50 km (Poulain, Warn-Varnes, and Niiler, 1996)

The grid size of a model should ideally be $\frac{1}{10}$ of the Rossby radius of deformation (Røed and Fossum, 2004). Smaller gyres can not be simulated if the resolution is too coarse (Poulain, Warn-Varnes, and Niiler, 1996).
The depth in the Svinøy section is approximately 500 m giving a $R_d \approx 450$ km. Since the resolution of the model near shore is < 45 km, eddies should be detectable in this region.
At the LB the depth is approximately 3000 meter resulting in a $R_d \approx 1400$ km. The models resolution off shore is < 140 km, so the quasi-permanent eddy in the basin should also be observable.

2.8.2 Eddy Heat flux

The observations of eddy heat fluxes are sparsely and notoriously difficult to determine. The fluxes usually consist of 2 components: a dominating rotational component, which does not contribute to the eddy heat flux, and a divergent component. These are hard to separate, making it difficult to interpreted observed eddy heat fluxes. By focusing on the divergence of the eddy heat flux and bypassing the rotational component a good estimate can be made. This has proven to be very difficult with the MIKE data due to the irregular triangular grid.

The time mean eddy heat flux is calculated by equation 2.25 for both components of velocity and temperature.

$$\overline{\mathbf{u}'T'} = \overline{(\mathbf{u} - \overline{\mathbf{u}})\left(T - \overline{T}\right)} \tag{2.25}$$

The velocity and temperature are first decomposed into means and perturbations $\mathbf{u}' = \mathbf{u} - \overline{\mathbf{u}}$ and $T' = T - \overline{T}$ where the overbar represents the time average of the component and the prime represents the deviation (Isachsen, Koszalka, and LaCasce, 2012).

2.8.3 Eddy kinetic energy

The total kinetic energy in the ocean is given by $TKE = \frac{1}{2}\overline{(u^2 + v^2)}$.
This equation can be split into two components: Kinetic energy of the mean flow MKE, equation 2.26 and eddy kinetic energy EKE equation 2.27.
The EKE is related to the turbulent eddies whereas the MKE is associated with the relative steady major currents.

EKE tends to be largest where the mean circulation is strong, indicating that eddies derive their energy from mean circulations. The ocean kinetic energy is dominated by the kinetic energy produced by eddies. The belt of strong EKE correlate to the shallow flow of the NwASC (Koszalka et al., 2011).

The kinetic energy of the mean flow:

$$MKE = \frac{1}{2}\left(\overline{u^2} + \overline{v^2}\right) \tag{2.26}$$

and the eddy kinetic energy:

$$EKE = \frac{1}{2}\overline{(u'^2 + v'^2)} \tag{2.27}$$

Chapter 3

Results

The data obtained from MIKE has been analysed in regards to velocity, transport, EKE, eddy heat flux, salinity and temperature in order to give an assessment of the currents in the NS.

3.1 Current velocity and direction

The Mike data for the current showed no spin up period, so the entire time-frame has been used for the calculation of the mean.

3.1.1 Mean flow

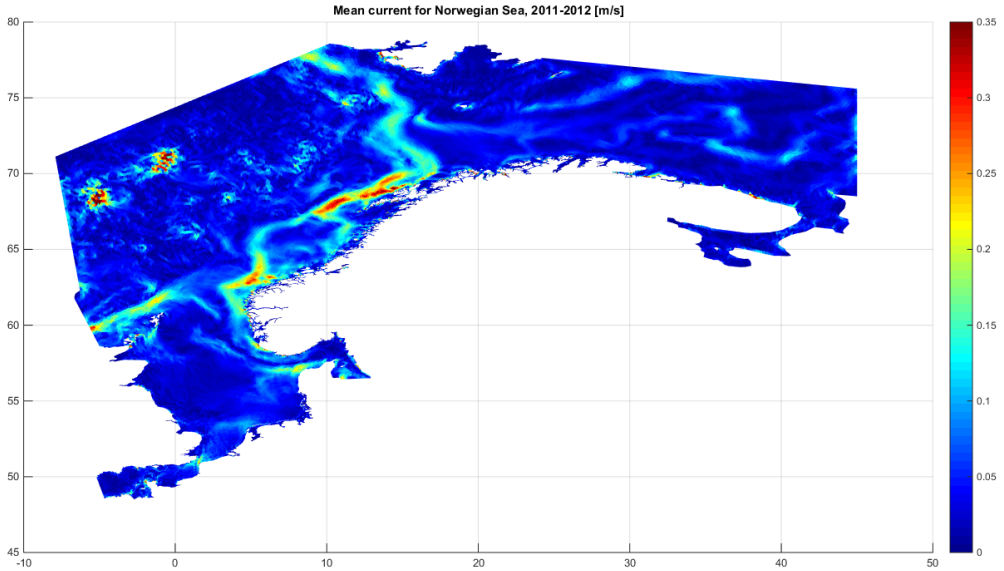

FIGURE 3.1: *Mean current velocity for the NS* $[\mathrm{m\,s^{-1}}]$.

The mean velocity for the NS is shown in figure 3.1. The structure of the currents is as expected with the high velocities following the topography.

The NwASC is especially visible coming into the NS between the Faroe Island and Shetland Island moving east towards Norway subsequently following the Norwegian shelf edge as it continues northward. After passing Lofoten the NwASC turns north-west for the Fram Strait.
The NwASC is strongest just west of Lofoten Island, with an area where the mean velocity reaches 0.4 $\mathrm{m\,s^{-1}}$, but also at the Svinøy section there is an area where mean velocity is strong $0.25 - 0.3\ \mathrm{m\,s^{-1}}$.

The NwAFC is harder to distinguish. The current generally has a lower velocity than the NwASC in the range of $20 - 25\ \mathrm{cm\,s^{-1}}$, but with the fairly still water surrounding the NwASC it should still be visible following the bathymetry of the Vøring plateau west of the NwASC.
According to earlier studies the NwAFC should have entered the NS at approximately $63°N$ and $5°W$.
There is a minor current velocity at this point at approximately 0.15 $\mathrm{m\,s^{-1}}$, far from the expected velocity of 0.25 $\mathrm{m\,s^{-1}}$ and there is no clear current path towards Norway. Further north there is still no indication of a strong current and no visual evidence of the topographical steering.

There is an increase in the velocity to 20 $\mathrm{m\,s^{-1}}$ at $70°N$, $5°E$, which corresponds well with the center of the LB and the activity of the quasi-permanent vortex, but it shows no vortex movement.

The NCC is also hard to determine. The current is noticeable at the south of Norway with a mean velocity of $0.15 - 0.20\ \mathrm{m\,s^{-1}}$ following the shoreline of Norway closely, but after it reaches the Svinøy section it is hard to identify it from the stronger NwASC. However there are indications of the NCC along the west coast of Norway on route towards Lofoten and with a mean salinity of 34.5 psu it is quite possible current water.

There are some anomalies found around the area of $10 - 0$ W and $67 - 72$ N. This is around the position of Jan Mayen which has not been included in the model except for a slight depth variation.

In figure 3.2 the data has been divided into bins of various velocities plotted against the model topography.
Here it is very evident that there exist a topographical steered current (NwASC). The expected mean velocity $> 30\mathrm{m\,s^{-1}}$ for the major currents is sparsely but exist in some areas.

Figure 3.3 and 3.4 shows the vectors of the direction of the current in the Svinøy section and Lofoten. The direction of the noticeable NwASC is, as assumed, parallel to the shore line following the bathymetry for the most part of the slope which is clear in both figures.

In figure 3.3 there is some inconsistency with the path of the NCC which seems to dissolve into the Lofoten Bay together with a small section of NwASC.
There are some indications of eddy activity around the green arrows in the LB.
In figure 3.4 the NwACS is primarily moving in the right direction with two areas of velocity $> 30\ \mathrm{m\,s^{-1}}$. Other wise the majority of the current velocity are in the range $10 - 20\ \mathrm{m\,s^{-1}}$.

Skagseth and Orvik (2002) found that the strongest current was located over the steepest part of the slope with a maximum of $30\ \mathrm{cm\,s^{-1}}$. This is visible in figure 3.4 and 3.3 where the red are arrows indicating $> 0.30\ \mathrm{m\,s^{-1}}$ are located in areas where the contour lines of the topography are close.

In general the structure of the mean velocity of NwASC is very alike the accepted structure for currents in NS as described in chapter 1.

3.1.2 Season variation of the currents in the Norwegian Sea.

Figure 3.5 shows the seasonal variation of the currents in NS for 2012.
There is a clear tendency to higher current velocity in the winter, figure 3.5a, and autumn, figure 3.5d, and a velocity minima in the summer, figure 3.5c. This can be caused by the stronger wind forcing that occurs in the the autumn/winter-time which for the model run was ~ 7 times greater in the winter than summer season, figure 3.6.

The general pattern of the currents path does not change noteworthy through the four seasons.

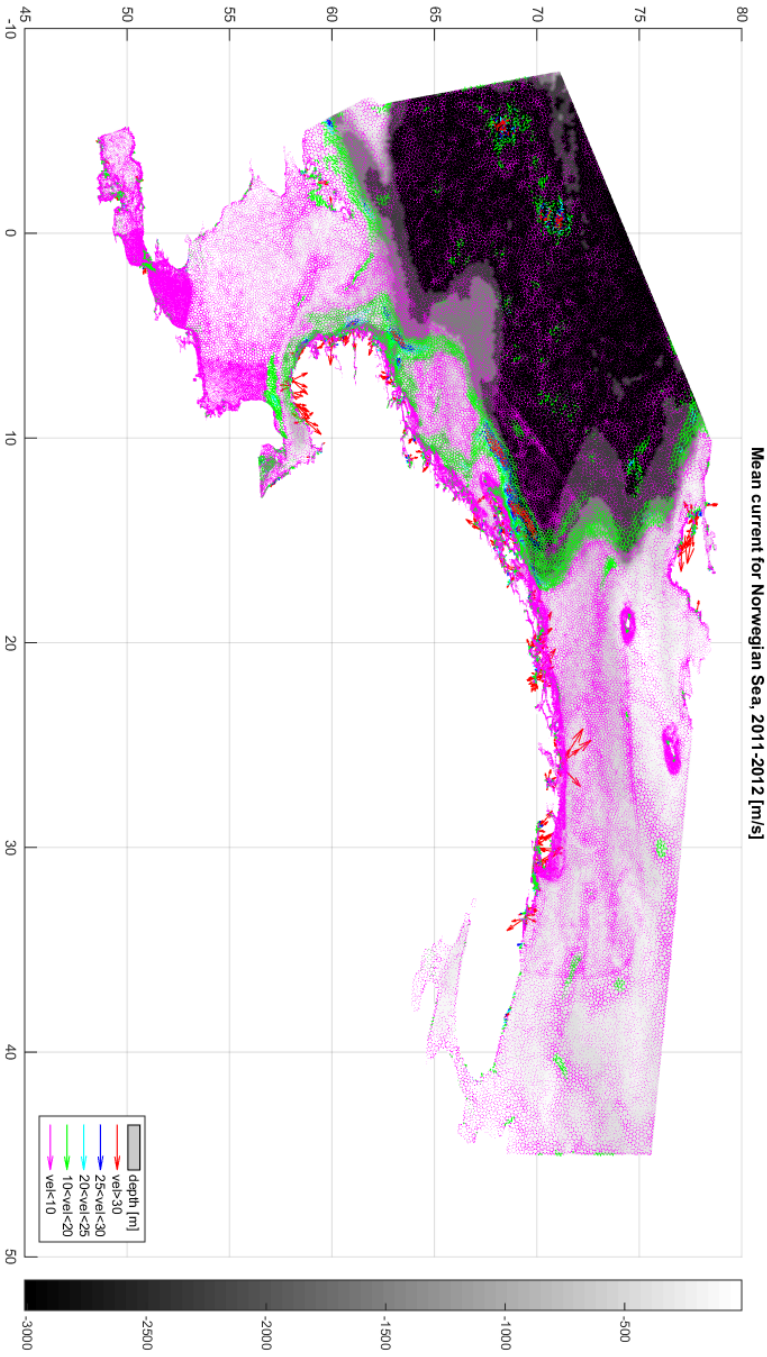

FIGURE 3.2: *Current following the contour of the ocean bed.*

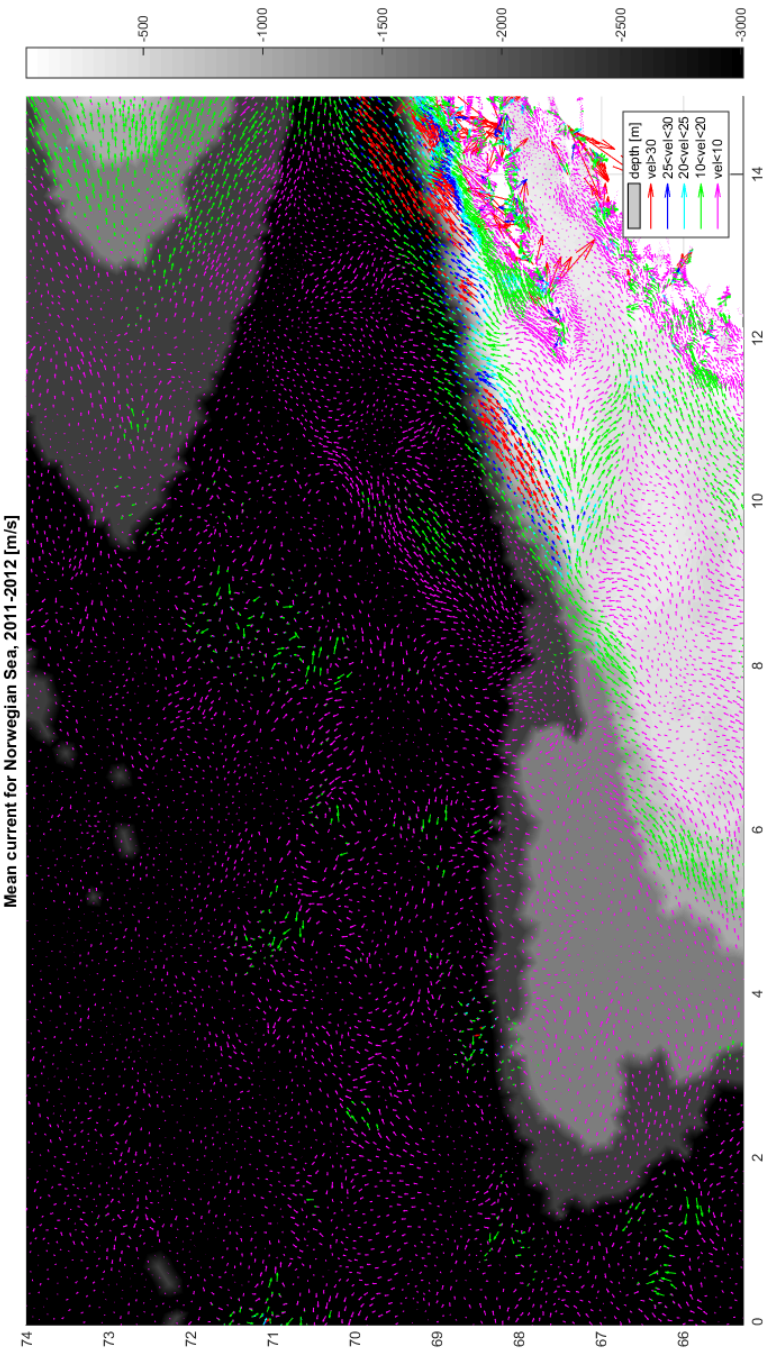

FIGURE 3.3: *The direction of the mean current in Lofoten.*

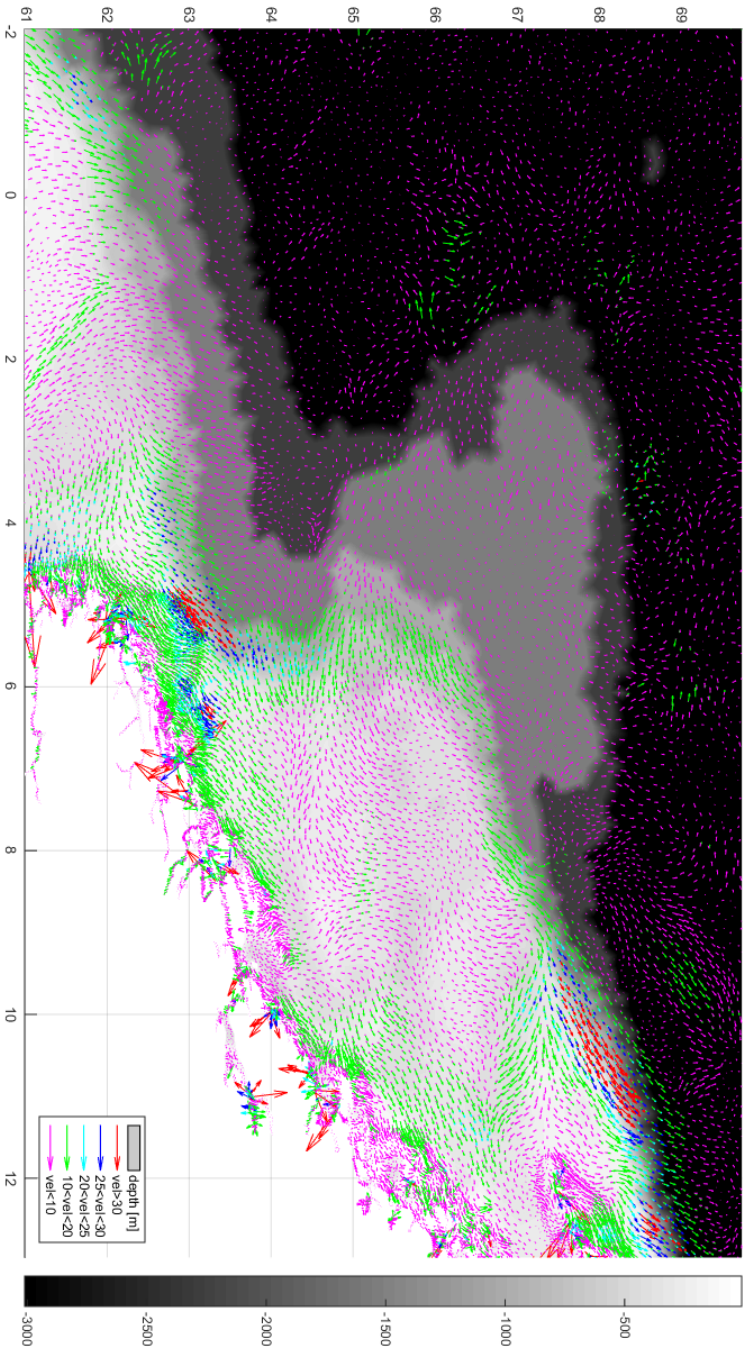

FIGURE 3.4: *The direction of the mean current at Svinøy.*

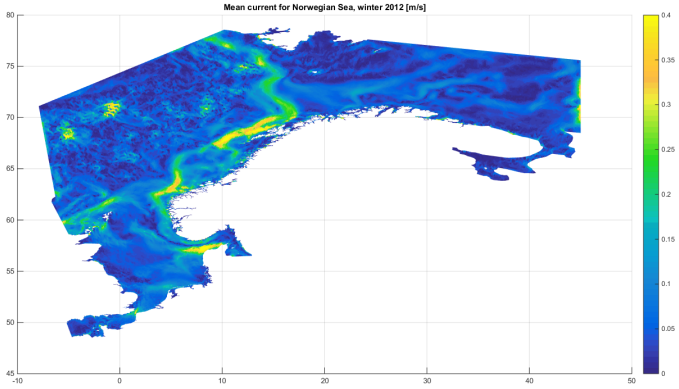

(A) *Winter mean current.*

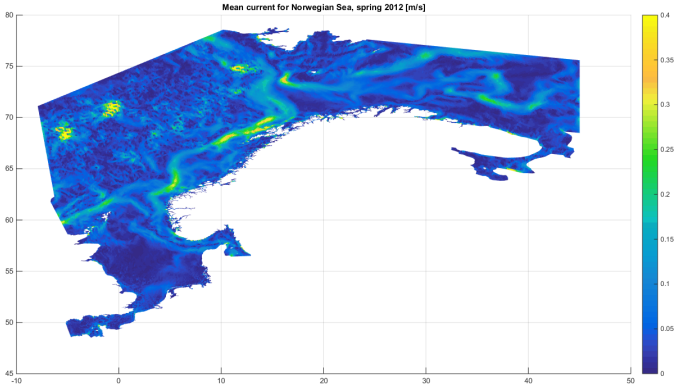

(B) *Spring mean current.*

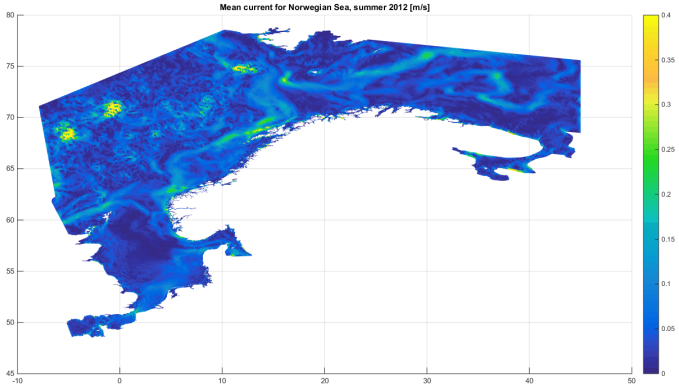

(C) *Summer mean current.*

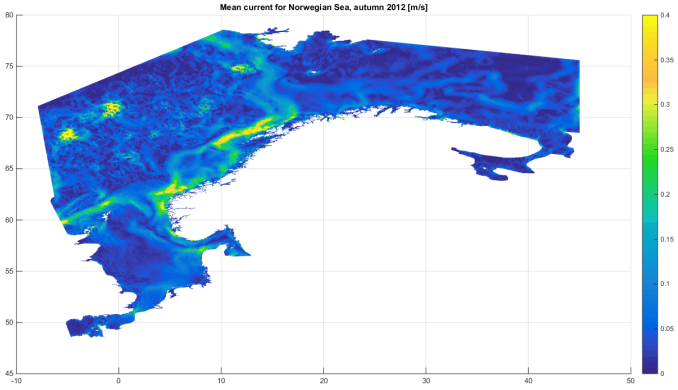

(D) *Autumn mean current.*

FIGURE 3.5: *The mean current for each season [$\mathrm{m\,s^{-1}}$] - 2012.*

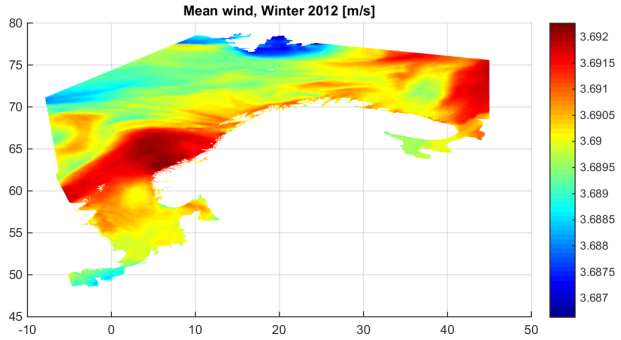

(A) *Mean wind velocity, winter.*

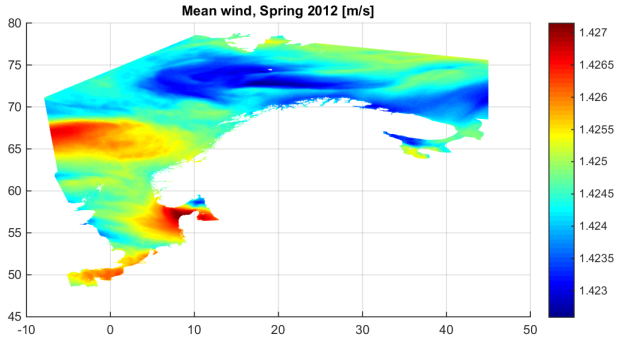

(B) *Mean wind velocity, spring.*

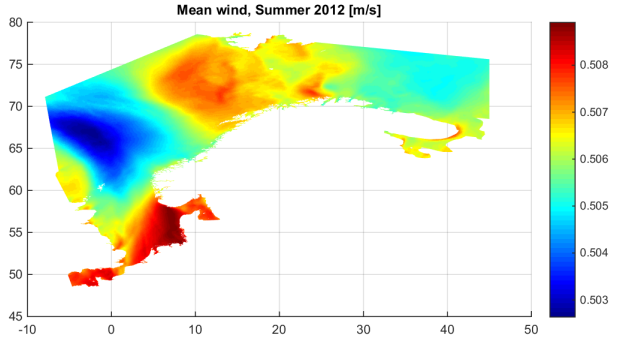

(C) *Mean wind velocity, summer.*

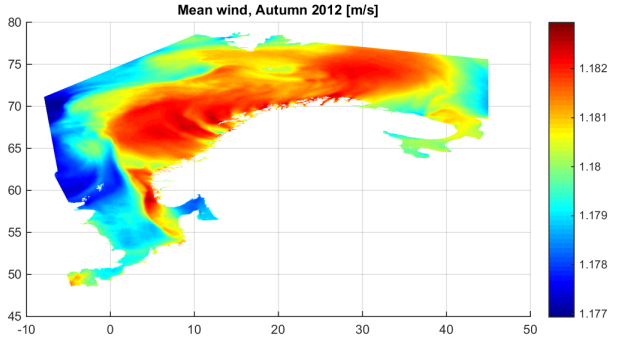

(D) *Mean wind velocity, autumn.*

FIGURE 3.6: *The difference between wind velocities at various seasons - 2012.*

3.2 Transport

The transport of water through the two sections can be viewed in figure 3.7, Svinøy section, and 3.8, Lofoten.

The top figure shows how the variation of the mean velocity is distributed over the depth. The bottom figure shows the calculated transport per meter for all water masses based on the velocity of the entire section and the depth.

From figure 3.7 it is again evident, that the NwASC at Svinøy is topographical steered, the highest velocity is located just above the shelf, not penetration deeper than 400 m, similar to the position of high saline water in figure 3.10b.
Figure 3.8 shows a related pattern for the NwASC with highest velocity not entering water beneath the depth of the slope. There is an increase in the velocity at 5° which is the the center of the LB. The distance of 1° is $\sim$ 70 km. The quasi-permanent vortex residing in the LB is found to have a diameter of 150 km (Koszalka et al., 2011), so it is not clear if the increase in velocity is caused by the vortex, and no other indications of the vortex has been found.

The specific transport of the saline AW are shown in table 3.1. This only includes the velocity of water with a salinity $>$ 35 psu.
From autumn and on there is no indication of water with salinity $>$ 35 psu at Lofoten, hence no results available.
The transport of AW is almost twice as large in the winter compared to summer in the Svinøy section. At the Lofoten section the limited number of results makes it difficult to discover a seasonal tendency.

TABLE 3.1: *Calculated transport for Atlantic Water.*

Season	NwASC, Svinøy	NwASC, Lofoten
Mean 2011-2012	6.3 Sv	6.4 Sv
Winter 2011	7.2 Sv	13.4 Sv
Spring 2011	7.3 Sv	5.7 Sv
Summer 2011	4.0 Sv	0.2 Sv
Autumn 2011	6.4 Sv	NA
Winter 2012	7.3 Sv	NA
Spring 2012	7.5 Sv	NA
Summer 2012	4.2 Sv	NA
Autumn 2012	6.6 Sv	NA

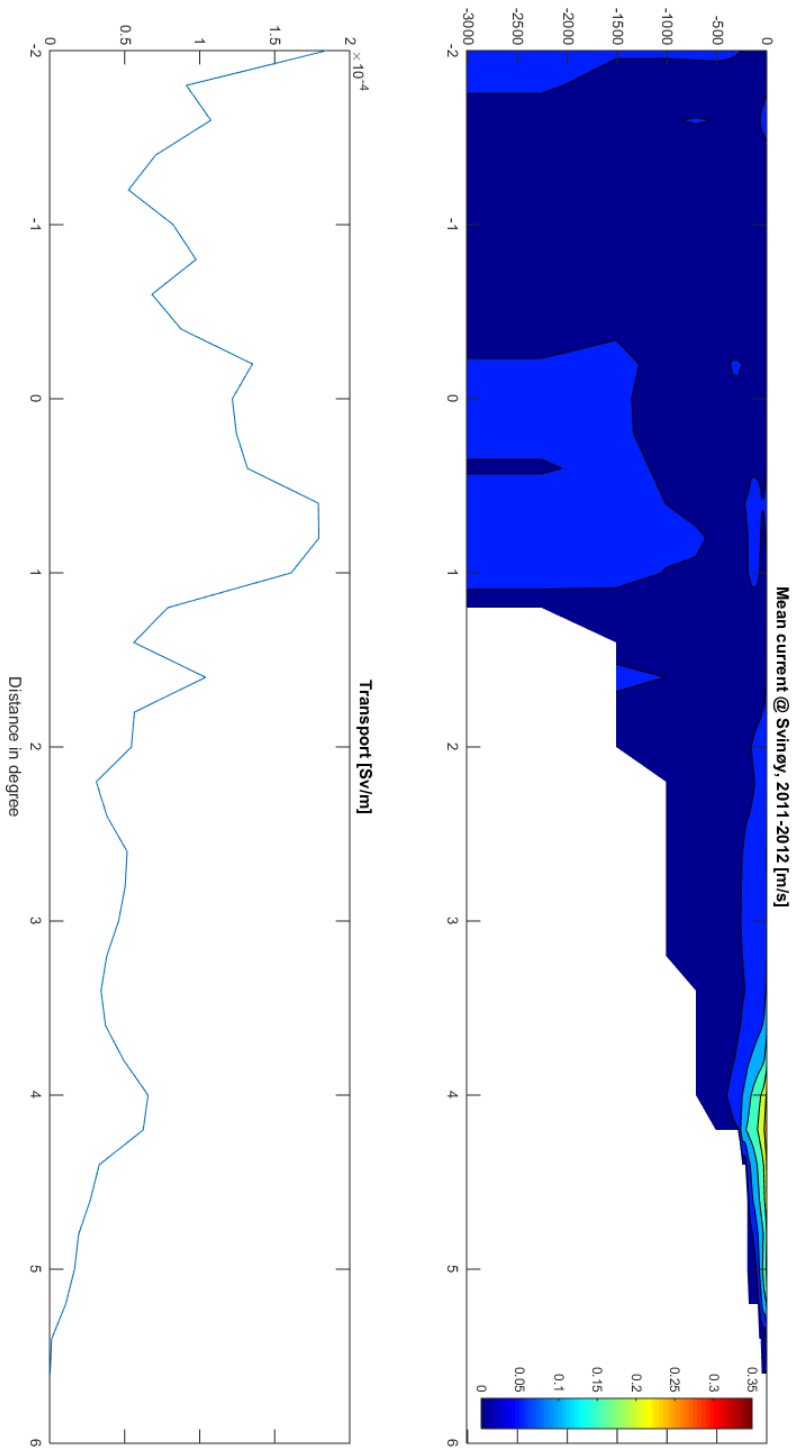

FIGURE 3.7: *Velocity and the related transport pr meter at Svinøy.*

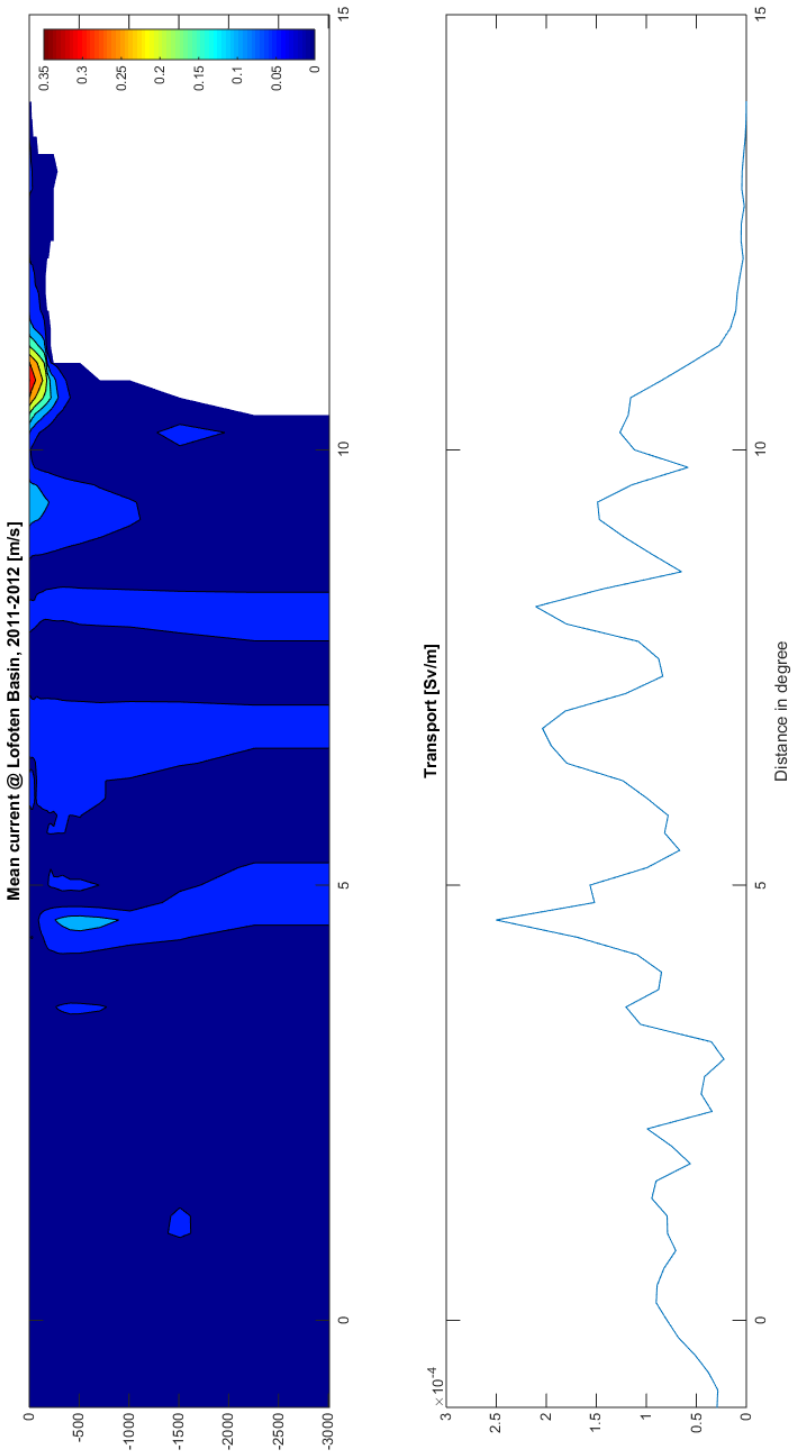

FIGURE 3.8: *Velocity and the related transport pr meter at Lofoten.*

3.3 Temperature and salinity.

Figure 3.9 shows how the warm AW enters the NS as a warm tongue of water steered by topography. The tongue is even wider and diffuse than the mean current, but the general structure is the same.
The change in the water temperature within the seasons are noticeable. The AW inflowing in the summer has a maximum temperature of $14 - 16°$ C and reaches mid Norway while the north is still dominated by cold water from the winter cooling.

The distribution of temperature and salinity through the two sections are displayed in the figure 3.10 for the Svinøy section and figure 3.11 for Lofoten.

The dark red areas in the salinity plot, figure 3.10b and 3.11b, indicates the presence of AW.

At the Svinøy section the warm water lies over the shelf as anticipated with a temperature in the range of $5 - 9°$ C which is the expected temperature for AW in this region, figure 3.12. The water temperature is highly dependent on season, with the warmest water in summer and autumn where the surface layers can reach temperatures of $> 14°$ C compared to winter and spring with surface temperatures around $6°$ C.

In figure 3.10b the characteristic wedge-shape of the high saline water is clearly visible over the shelf.

The saline field is not very depended on the season as seen in figure 3.13. The dispersion of the saline water is quite similar ranging from approximately $2E \rightarrow 4°40'E$ reaching the shelf at the deepest point at -1000 m. Only the salinity of winter has a slight difference. The wedge is more wide going from $1E \rightarrow 4°40'E$ and with a depth of -700 m.

The temperature range at Lofoten is somewhat colder, $4 - 8°$ C, which is in the high end of the expected temperature range. The summer/autumn season has the highest temperature here as well reaching $11°$ C with a winter/spring max temperature of $6°$ C, figure 3.14.

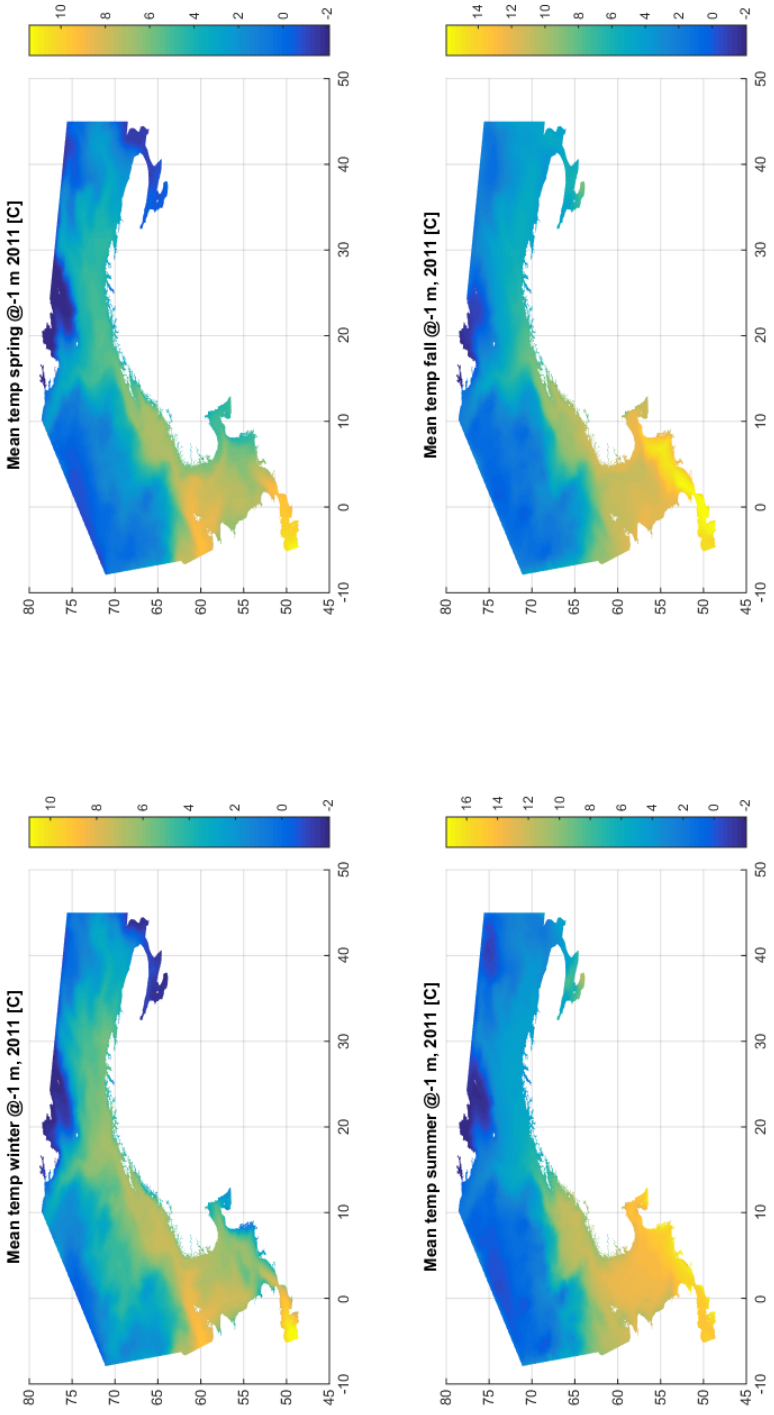

FIGURE 3.9: *Seasonal surface temperature in the Norwegian Sea.*

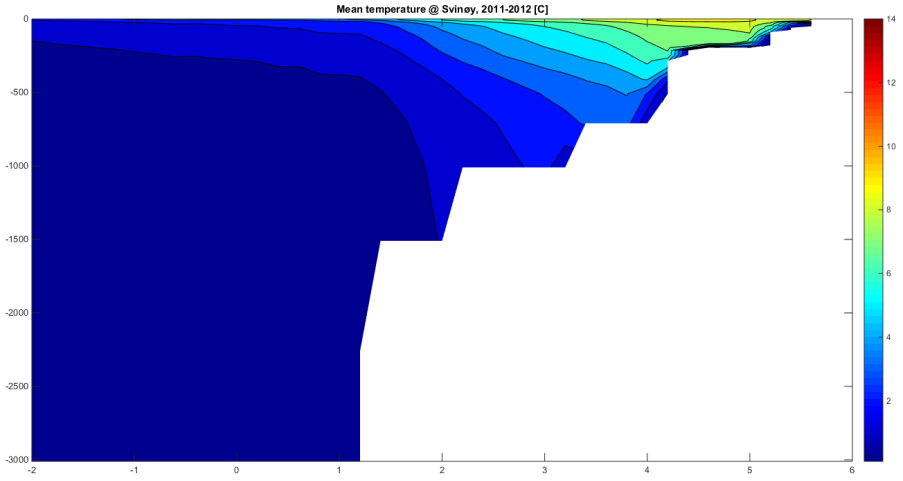

(A) *Mean temperature* [°*C*].

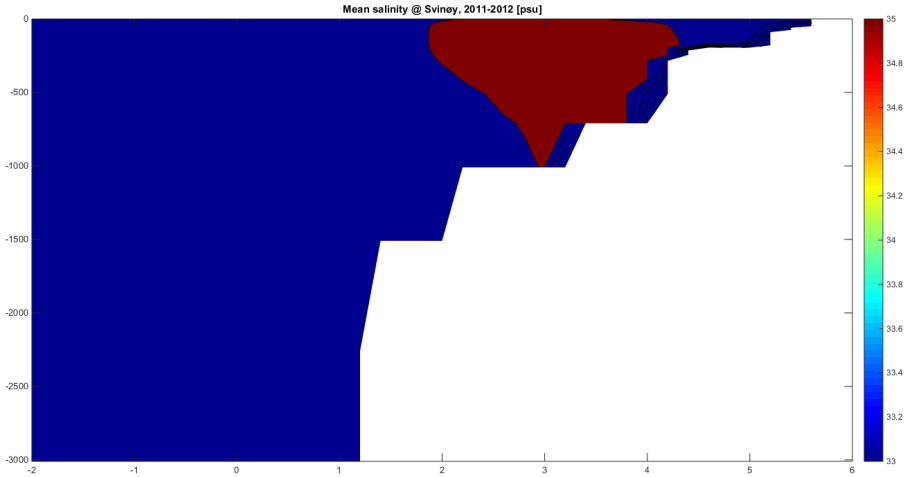

(B) *Mean salinity [psu].*

FIGURE 3.10: *Water composition, Svinøy 2011-2012.*

At Lofoten the salinity, figure 3.11b, indicates tant only a modest amount of AW reaches this section as a mean of the year.

The salinity here is highly variable. In the start of the model run, figure 3.15a, there is a very wide wedge stretching into the LB, almost reaching the far end of the basin at 1°5′. By spring the wedge has diminished significantly, and it does not enter the LB. By summer the amount of saline water is minuscule and by fall the final indications of AW at Lofoten has vanished and there are no indications of returning AW in the following seasons.

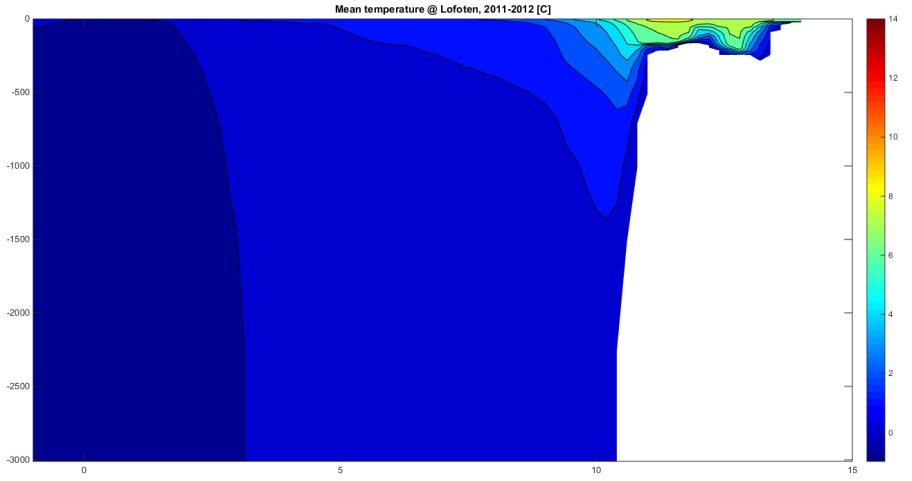

(A) *Mean temperature* [$^{\circ}C$].

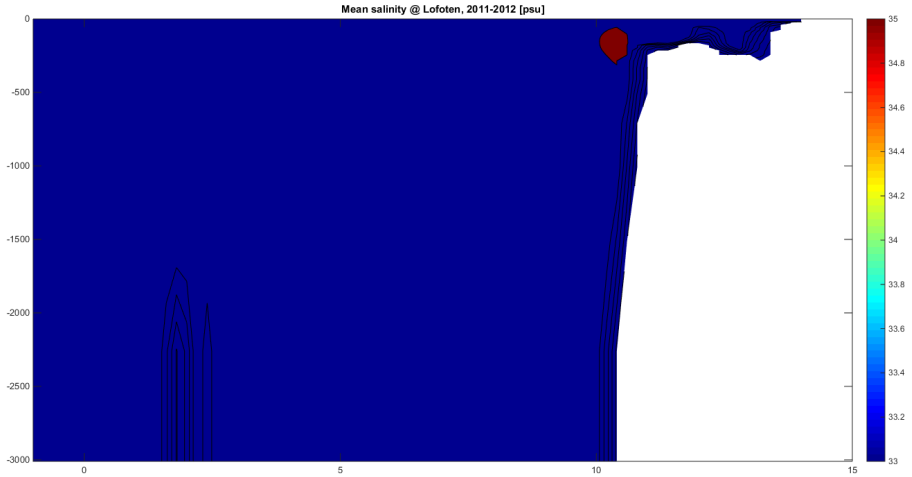

(B) *Mean salinity [psu].*

FIGURE 3.11: *Water composition, Lofoten 2011-2012.*

For both sections the warm water stays above the shelf and does not descent below 300 m.

When looking at the distribution of warm water and high salinity, there is a clear pattern. When the salinity wedge is wide, so it the wedge of warm water. This is especially clear at Svinøy.

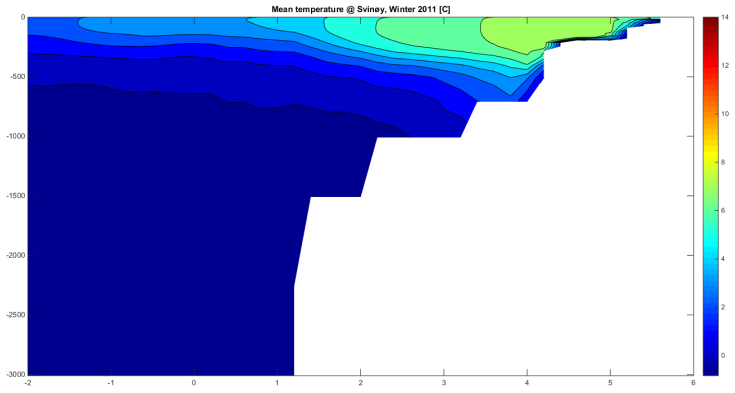

(A) *Winter.*

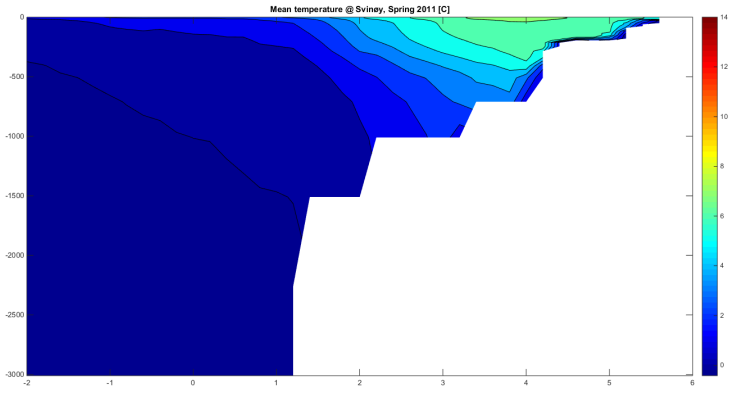

(B) *Spring.*

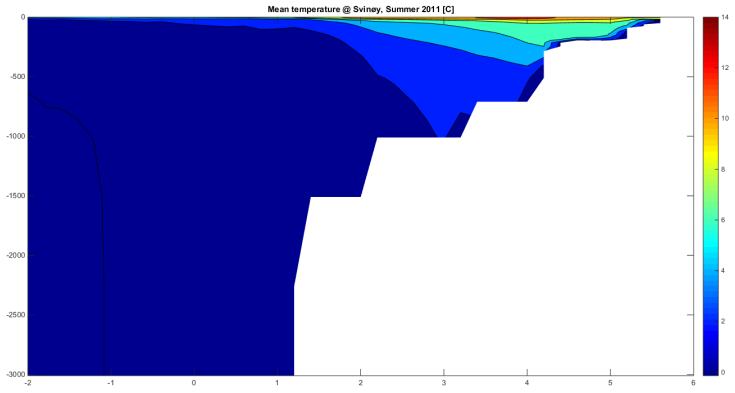

(C) *Summer.*

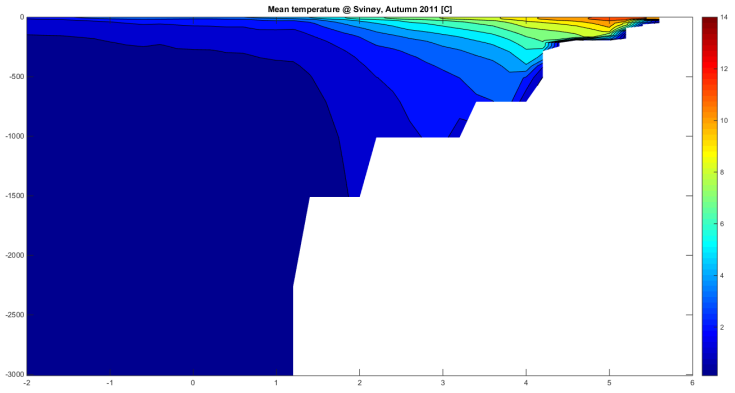

(D) *Autumn.*

FIGURE 3.12: *The mean temperature for each season at Svinøy - 2011.*

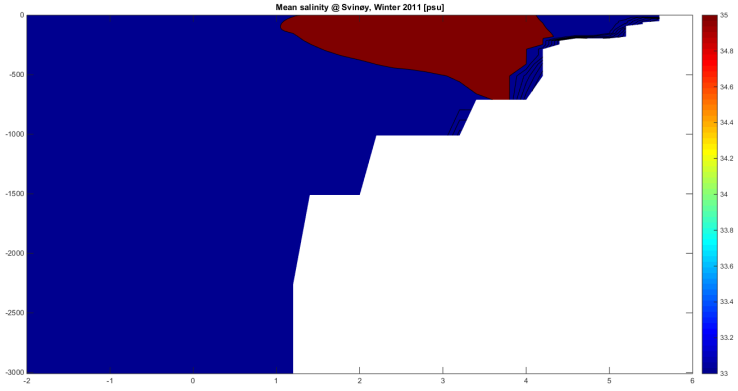

(A) *Winter.*

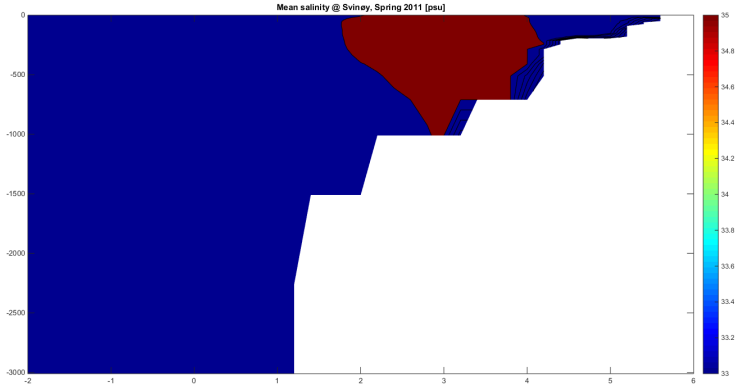

(B) *Spring.*

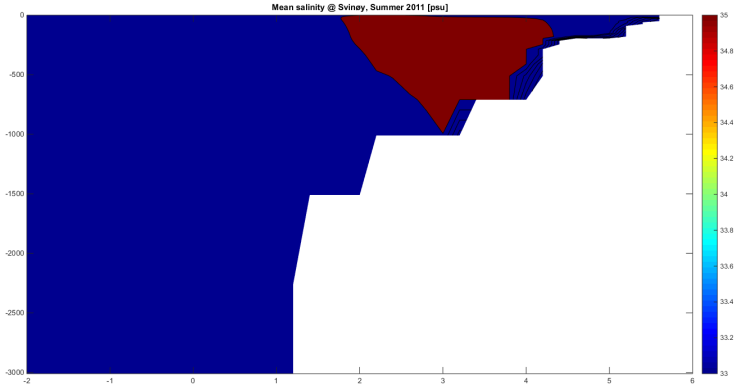

(C) *Summer.*

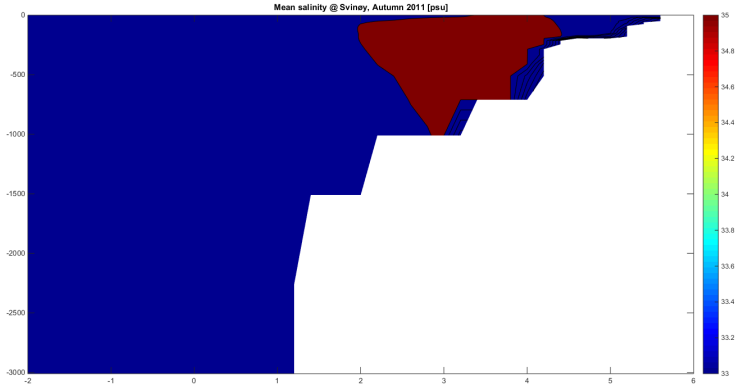

(D) *Autumn.*

FIGURE 3.13: *The mean salinity for each season at Svinøy - 2011.*

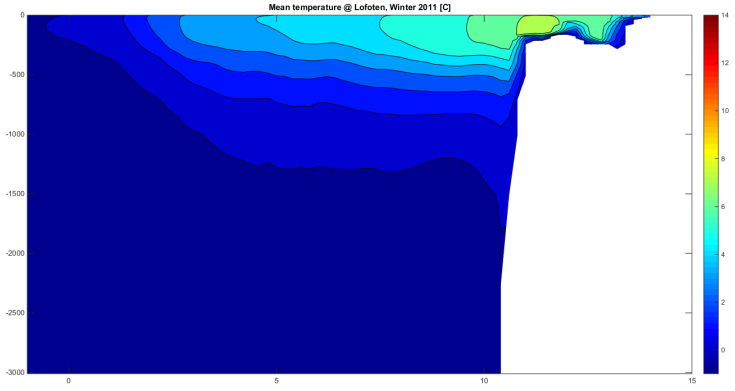

(A) *Winter.*

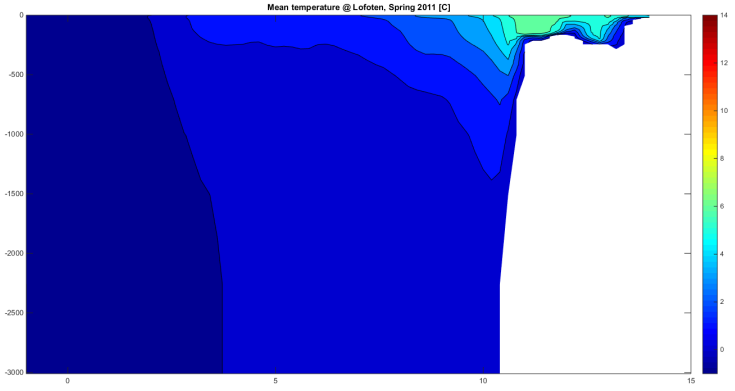

(B) *Spring.*

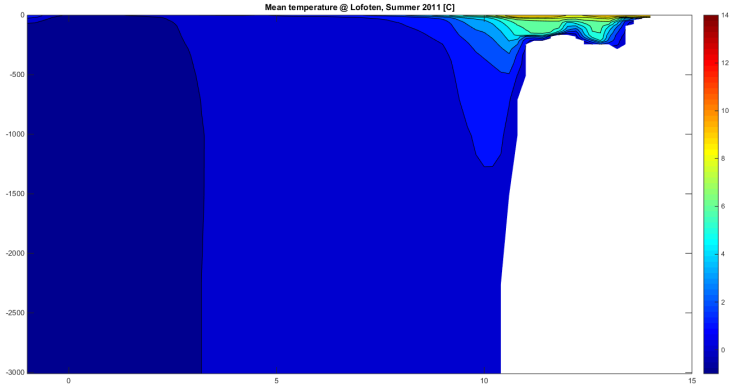

(C) *Summer.*

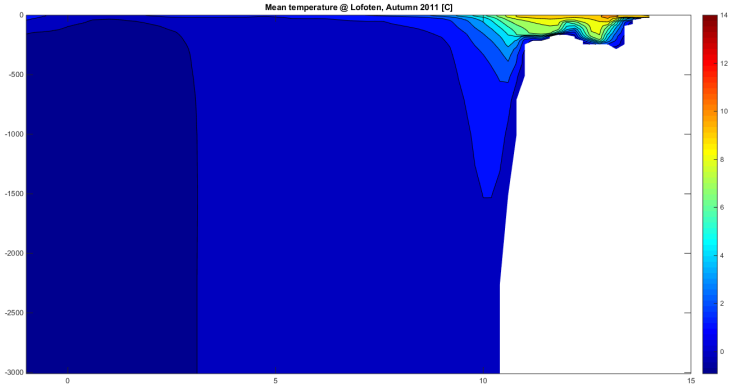

(D) *Autumn.*

FIGURE 3.14: *The mean temperature for each season at Lofoten - 2011.*

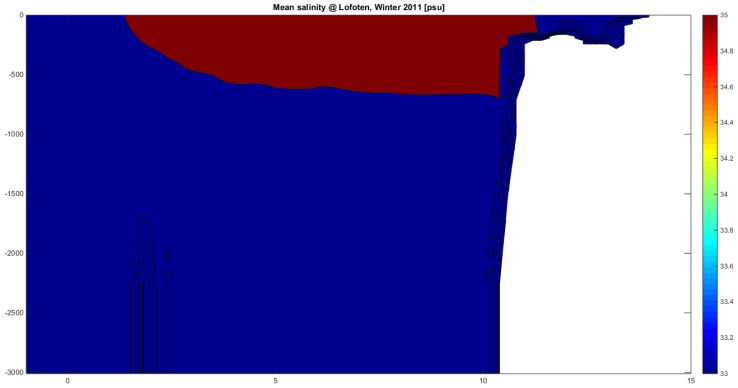

(A) *Winter.*

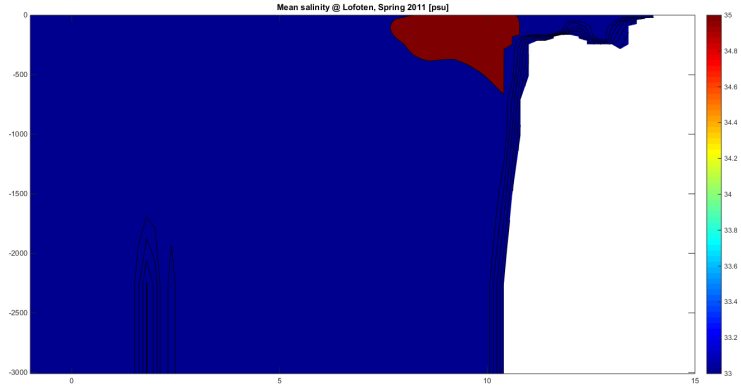

(B) *Spring.*

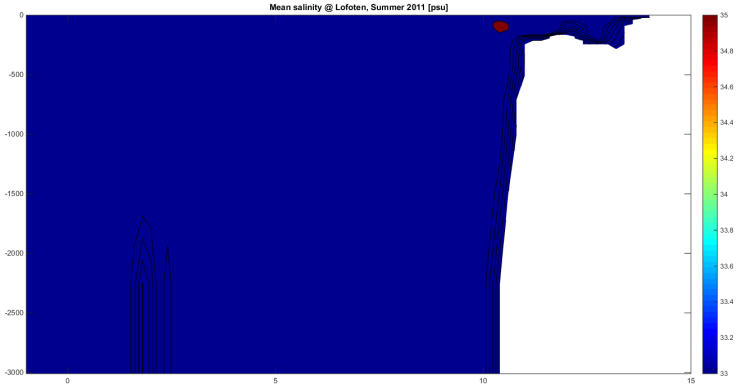

(C) *Summer.*

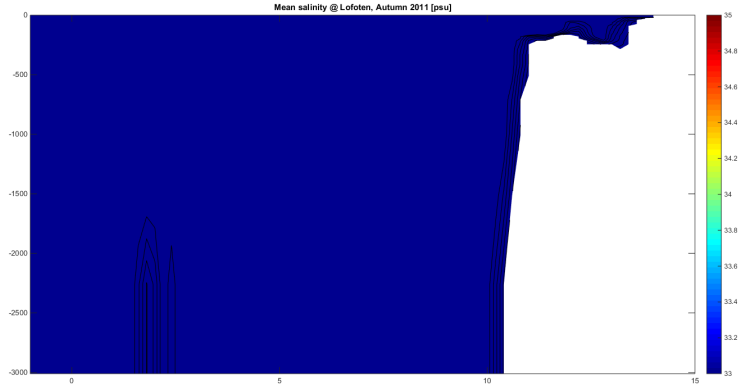

(D) *Autumn.*

FIGURE 3.15: *The mean salinity for each season at Lofoten - 2011.*

3.4 Eddy

The model data does not reveal any clear evidence of the quasi-permanent vortex in the LB, the velocities in this area are simply to low.

3.4.1 Eddy heat flux

The magnitude of the mean eddy heat flux is shown in figure 3.16a for the surface and figure 3.16b for 15 m depth.

The largest heat flux occurs near Svinøy at the surface with a maximum of 0.25 C·m s^{-1}.

The heat flux is fairly aligned with the bathymetry and the overall shape is quite similar to the shape of the current, and declines in magnitude at deeper depths.

Figure 3.17 shows the direction of the heat flux in the northern part of Norway including the LB. There are no indications of heat being transferred into the LB and the mean direction for the heat flux is unexpected south-east. This also applies for the mean direction of heat flux in the south, figure 3.18.

In order for the heat to be transported northward the mean eddy induced heat transport should be in the direction of north to north-east.

Since the eddy heat flux is dependent on the current velocity and the temperature which both vary greatly with season as shown earlier, the seasonal variation of the heat flux has also been studied.

Seasonal variation

The magnitude of the seasonal variation for 2011 is shown in figure 3.19. The strongest heat flux occurs in the autumn. In this period the velocity is increasing due to increasing wind forcing and the water is still warm from the summer heating.

The direction of heat flux for each season has been found from plots. The direction for autumn 2012 is shown in figure 3.20 and 3.21. The variation of the

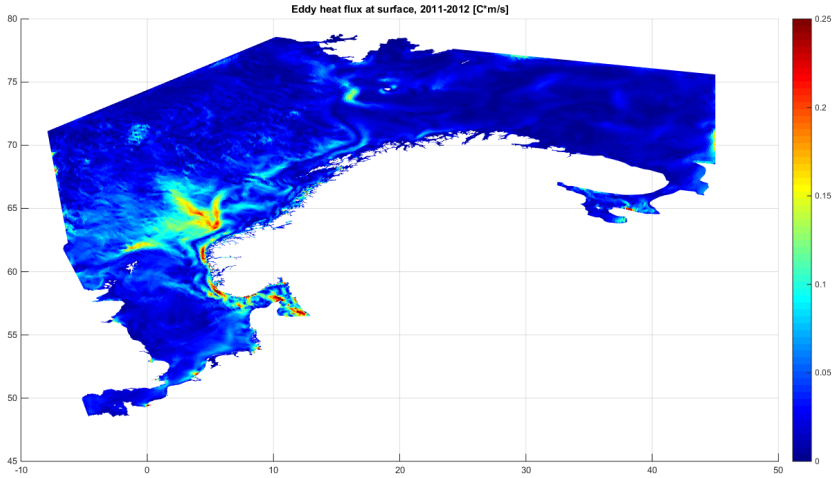

(A) *Surface.*

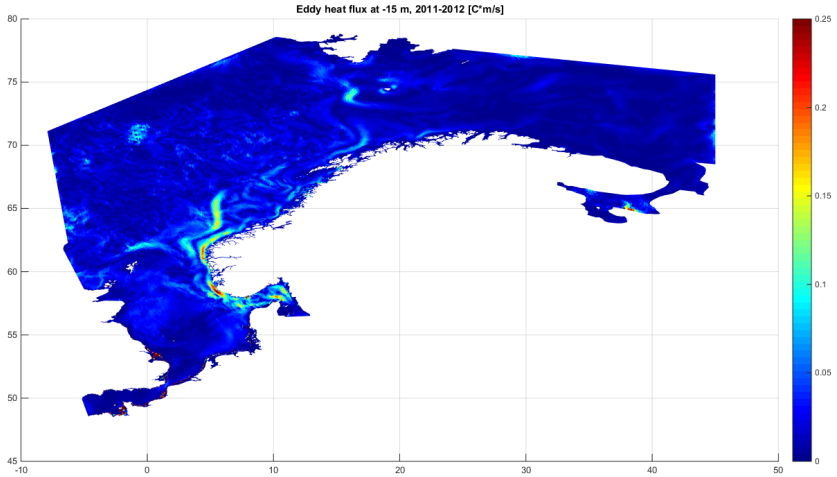

(B) *-15 m.*

FIGURE 3.16: *Eddy heat flux 2011-2012.*

general direction for all the seasons is shown in table 3.2. S indicates south direction, N = north, W =west and E = east.

The direction of the heat flux shows a tendency of south to south-west in the winter and spring time, where it is colder and north-east in summer and fall when the water is warmer.

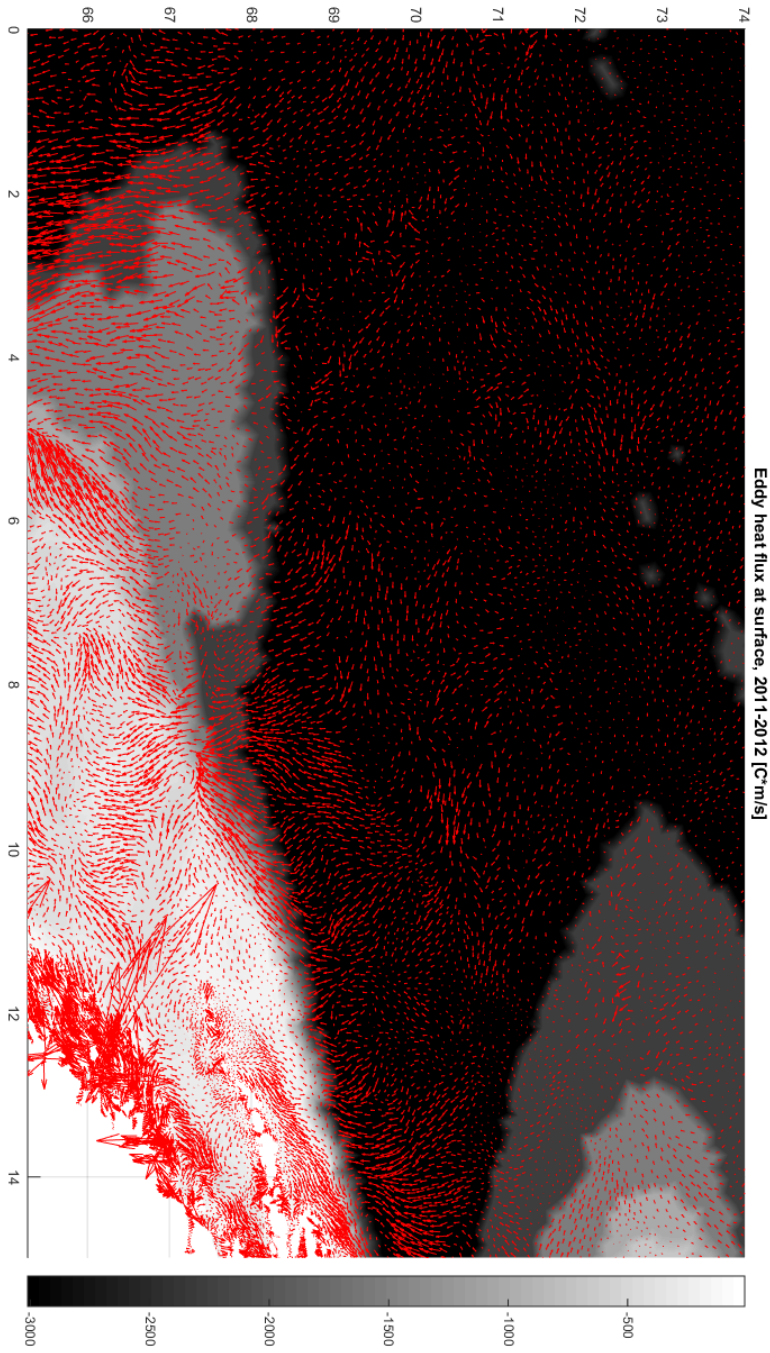

FIGURE 3.17: *Eddy heat flux at Lofoten.*

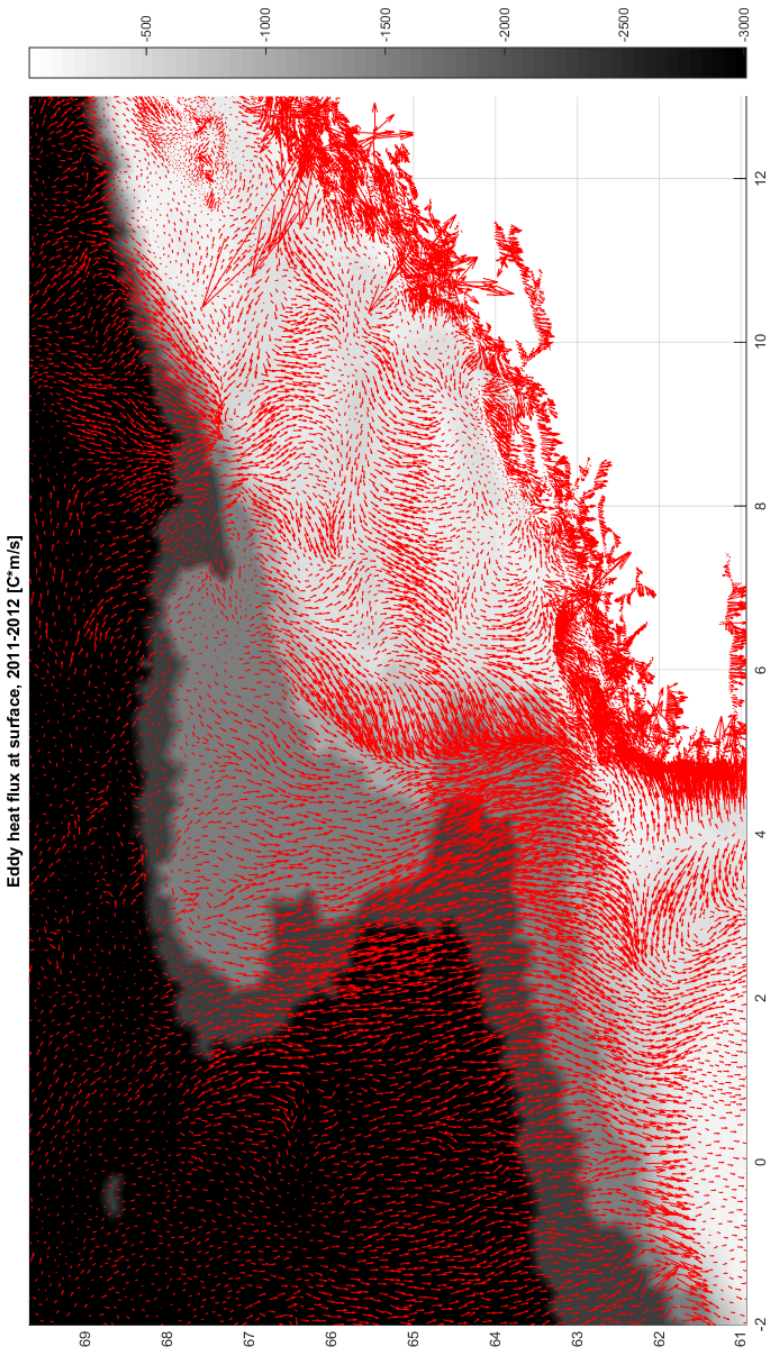

FIGURE 3.18: *Eddy heat flux at Svinøy .*

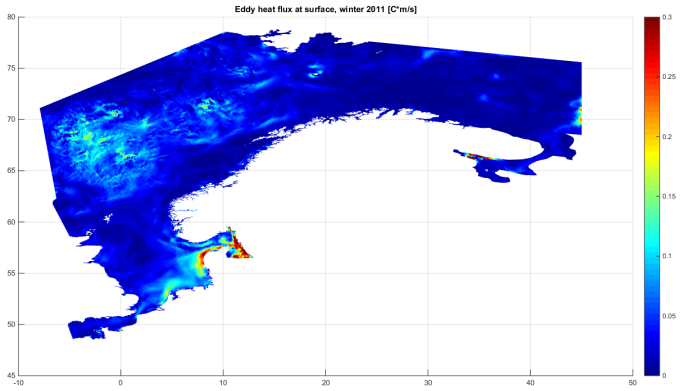

(A) *Winter.*

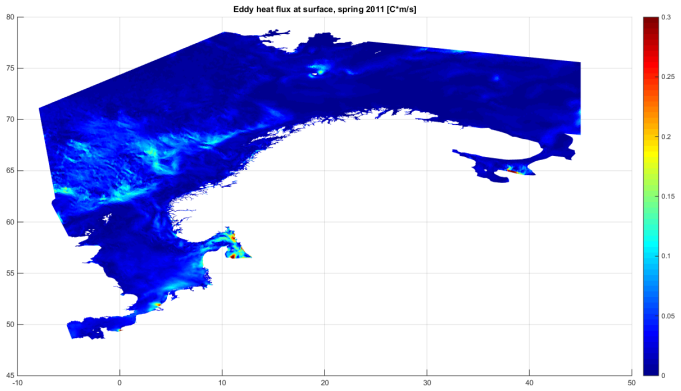

(B) *Spring.*

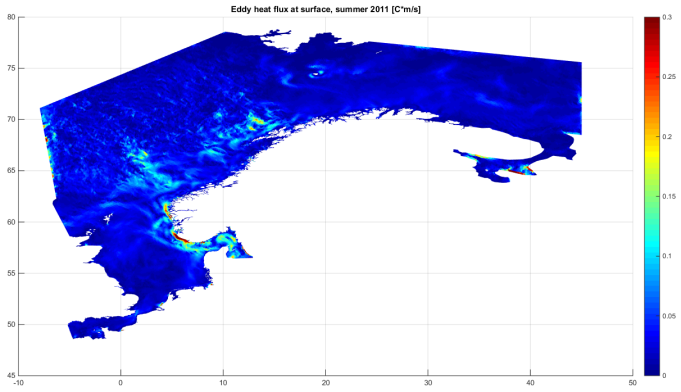

(C) *Summer.*

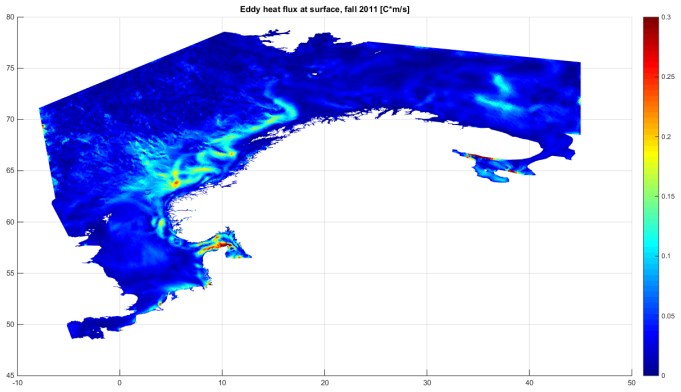

(D) *Autumn.*

FIGURE 3.19: *Eddy heat fluxes for the seasons - 2011.*

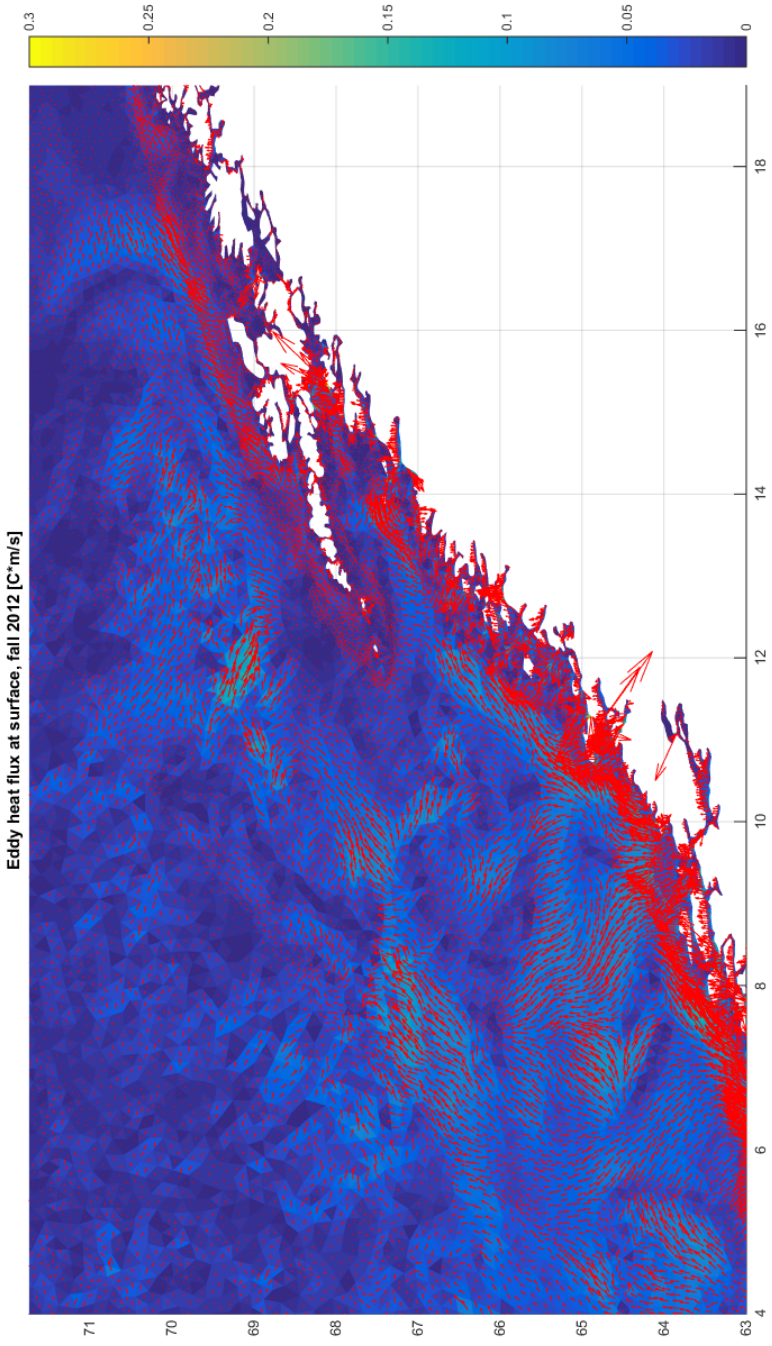

FIGURE 3.20: *Eddy heat flux in northern Norway, Autumn 2012.*

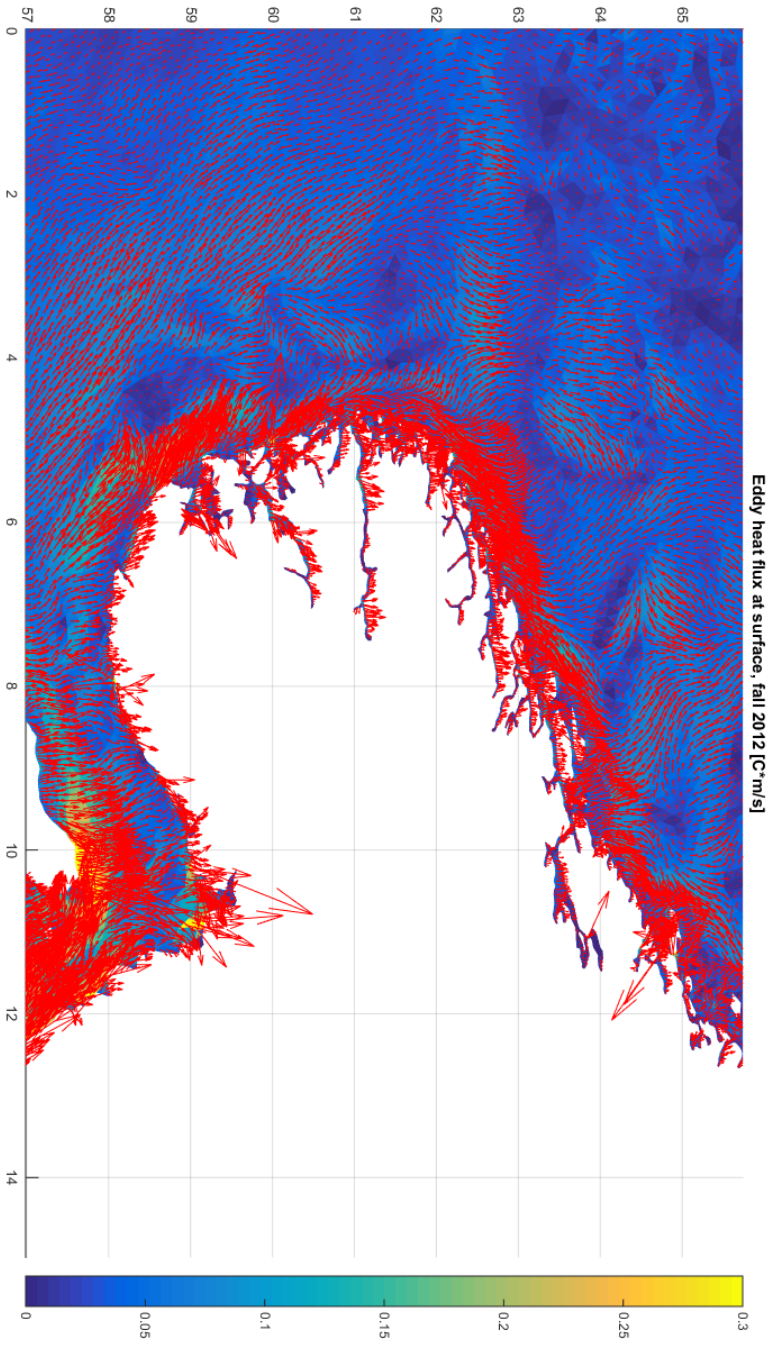

FIGURE 3.21: *Eddy heat flux in southern Norway, Autumn 2012.*

TABLE 3.2: *Direction of Eddy heat flux at various seasons in the northern and southern Norway.*

	2011		2012	
Season	North	South	North	South
Winter	S-W	S-W	E	N-E
Spring	S	S	S	S
Summer	N-E	S	N-E	N-E
Autumn	S-W	S-W	N-E	N-E

3.4.2 Eddy Kinetic Energy

The mean EKE for the model is shown in figure 3.22.

There is an area of large EKE along the path of NwASC at the south of Norway near Svinøy and and an even larger at Lofoten with a maximum 0.06 m^2/s^2 showing that the largest EKE occurs where the mean current velocity is strongest. There is no regions outside the slope current showing evidence of eddy activity.

Season variation

The EKE clearly follows the bathymetry an the NwASC in all seasons and there is a clearly enhanced EKE west of Lofoten at all seasons, figure 3.23.
Similar to the current velocity the strongest EKE is found in the winter/autumn, where values > 0.06 m^2/s^2 covers larger parts of the slope.
In the summer the EKE is at its lowest with a mean of 0.03 m^2/s^2.

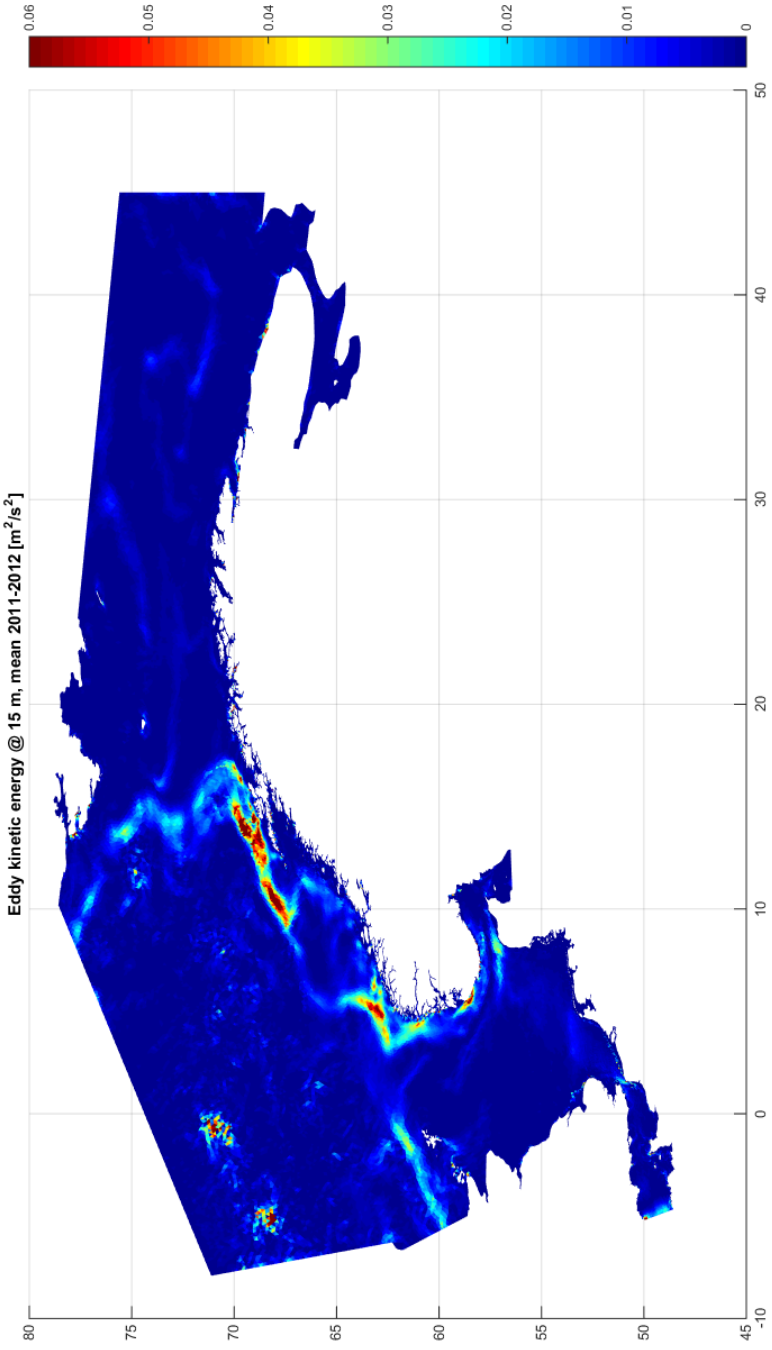

FIGURE 3.22: *Mean eddy kinetic energy at 15 m 2011-2012.*

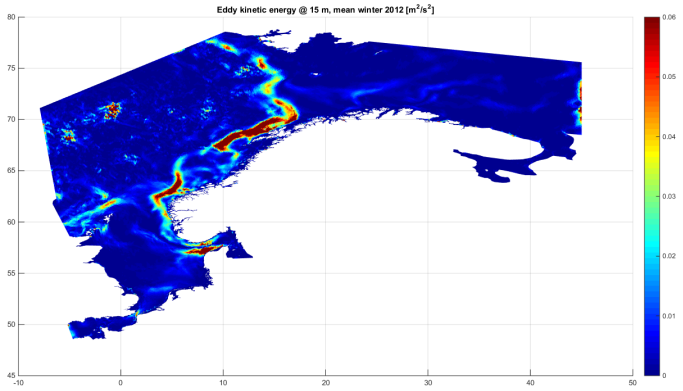

(A) *Winter.*

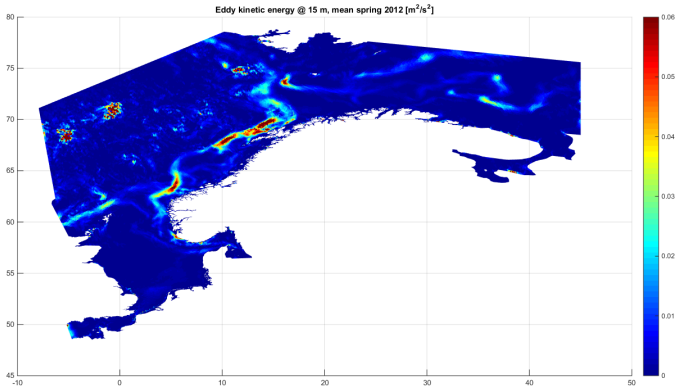

(B) *Spring.*

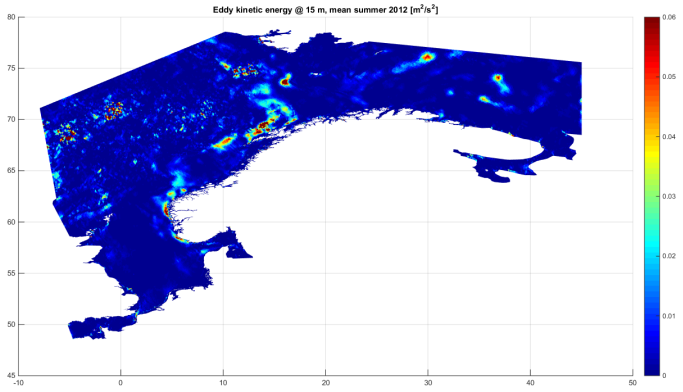

(C) *Summer.*

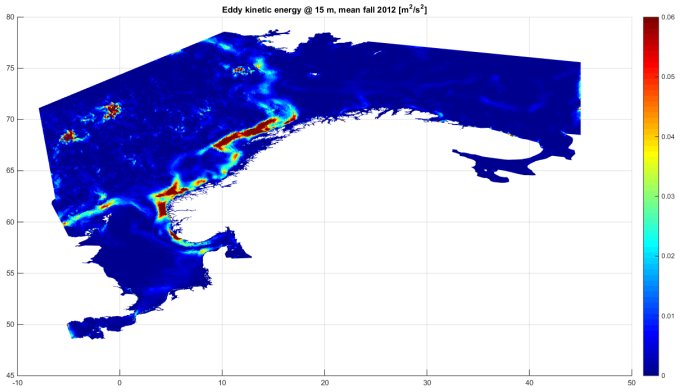

(D) *Autumn.*

FIGURE 3.23: *Eddy kinetic energy for the seasons - 2012.*

Chapter 4

Discussion

The aim of this study was to evaluate how well the data from the MIKE model represented the NS regarding current, transport, eke, heat flux, salinity and temperature.
The modelled results will be compared with earlier surveys and models.

4.1 Current

In the MIKE model the best represented current is the NwASC.

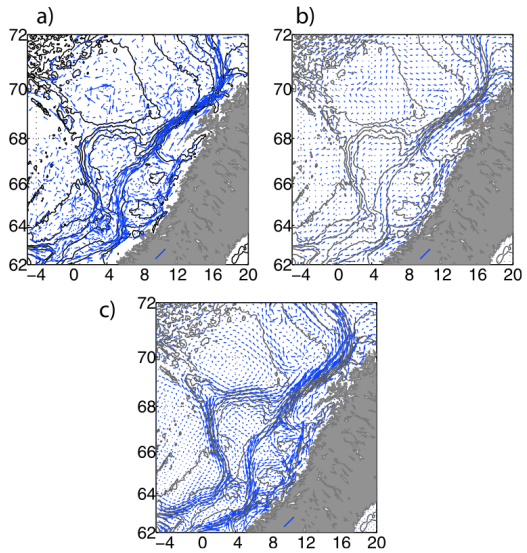

FIGURE 4.1: *Mean surface current from a) drifters, b) altimeter observations and c) model (Isachsen, Koszalka, and LaCasce, 2012).*

The pathway is clearly topographically steered as predicted and even though the mean current velocity is not 0.30 $\mathrm{m\,s^{-1}}$ throughout it still consist of some high velocity areas.
If compared to the estimated surface currents found by (Isachsen, Koszalka, and LaCasce, 2012), figure 4.1, there is a very good conformity between them, especially the path of NwASC is very similar and the velocity is in the same range even though result from the MIKE model is in the low end.

The path of the NCC in MIKE and figure 4.1 is also quite comparable, but here the difference in the magnitude of

the velocity is noticeable with the drifter data providing a mean of 0.25 $\mathrm{m\,s^{-1}}$ compared to the MIKE data with a mean velocity of 0.25 $\mathrm{m\,s^{-1}}$.

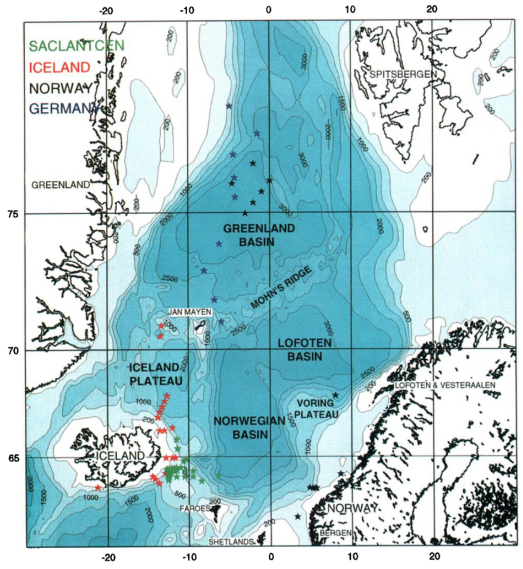

FIGURE 4.2: *The Bathymetry of the Nordic Sea (Poulain, Warn-Varnes, and Niiler, 1996).*

A big issue with the MIKE model is that there is no indications of the NwAFC.
A reason for this could be that the model is overly sensitive to the bathymetry, and thereby does not steer the AW into the two separate currents but rather combine them in one.

The bathymetry used in the MIKE model, figure 4.3, is well defined along the continental slope with depths at around 500 m. The Vøring Plateau is also easily recognisable going down to 1500 m, but for the deeper ocean, the ridges dividing the different basins are omitted.
Especially the Mohn's Ridge as seen in figure 4.2 is not defined.
It is this acclivity of ocean bottom combined with the Vøring plateau which is thought to be the reason the NwAFS is guided from Svinøy to the left of LB and further towards the Fram strait (Orvik, Skagseth, and Mork, 2001).

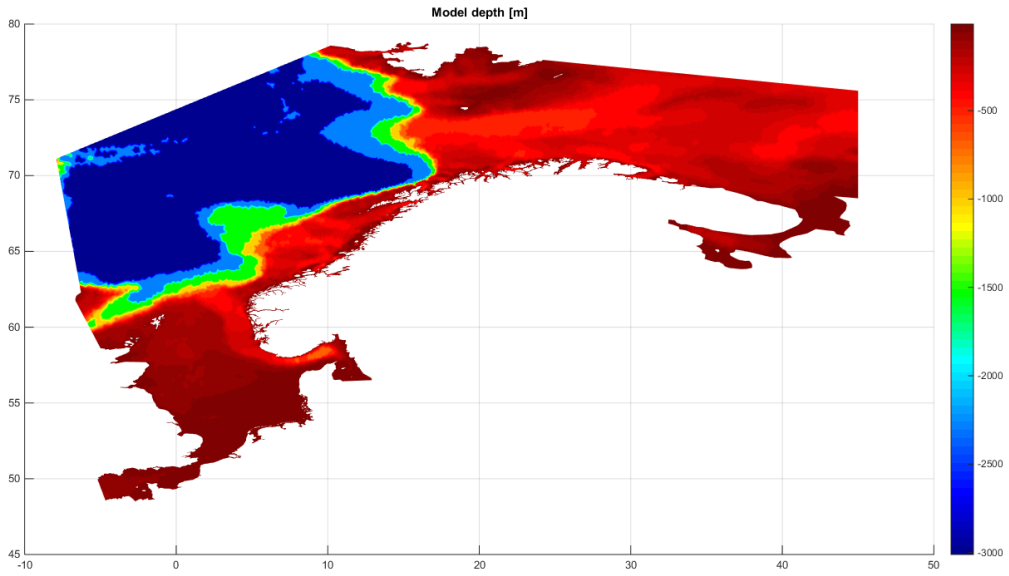

FIGURE 4.3: *The Bathymetry used in generating the MIKE data.*

Isachsen et al. (2003) found that the circulation in the NS is intensified during the winter period as a result of greater wind forcing which would drive a stronger flow.

The MIKE model shows a clear tendency for a greater current velocity in the autumn and winter period, and combined with the similar change in the wind forcing this is accurate for the model as well.

Orvik and Skagseth (2005) also found evidence of a link between the variation of the current flow and the wind field, where monthly variation appeared as a direct response to the large scaled wind fields while inter-annual variations was driven by the wind stress curl in the North Atlantic Ocean.

The large velocities of the current does not decent further than the slope at around $\sim$ 400 m. This is in accordance with the finding by Mork and Blindheim (2000) who determined that the large velocities did not surpass 600 m.

From the models current data it could look like the location of AW inflow to the NS might have something to do with the circulation in the model.
Changing the parameters allowing another inflow between Iceland and Faroe Island could prove to provide the necessary force to power the NwAFC.

4.2 Transport

The ongoing survey at the Svinøy section have since 1995 provided several estimates of the AW transport through this section as shown in table 4.1.

The earlies recorded transport was made by Helland-Hansen and Nansen (1909) and does not cover the exact Svinøy section but the area around the south of Norway.

TABLE 4.1: *Transport of Atlantic Water in The Norwegian Sea at the Svinøy section.*

Source	NwAFC	NwASC	Total
(Helland-Hansen and Nansen, 1909)	-	3.8 Sv	-
(Mork and Blindheim, 2000)	-	-	5.6 Sv
(Orvik, Skagseth, and Mork, 2001)	3.4 Sv	4.2 Sv	7.6 Sv
(Orvik and Niiler, 2002)	-	3.5 Sv	-
(Skagseth, 2004)	3.5 Sv	4.5 Sv	8.0 Sv
(Mork and Skagseth, 2010)	3.4 Sv	1.7 Sv	5.1 Sv
MIKE model 2011-2012	-	6.3 Sv	-

The mean transport calculated from the model data is in the high end of the range for NwASC transport, but assuming that the topography is driving the two currents together, the total transport would be in the range of earlier estimates.

Mork and Skagseth (2010) had earlier concluded that the estimated transport did not show any systematic seasonal variation, but later they found evidence of a winter maxima almost twice the amount compared to the summer minima, thereby determining that the transport in NS was subjected to a systematic annual cycles.

Looking at the seasonal transport for Svinøy the same tendency is clear. The highest transport occurs in the winter and spring period with a transport of ~ 7.3 Sv compared to the summer low at ~ 4.1 Sv.

The few transport calculations from Lofoten gave a mean transport of 6.4 Sv, which is in accordance with the calculated transport by Orvik (2004), who found the volume transport for the NwASC at Lofoten to be about 5 Sv.
However, the variation of the transport in Lofoten over the three months where AW were present, is too great to make a certain conclusion.

It is worth to notice, that even though the current velocity, found by the model data, is lower than the mean velocity from measurements, the transport for the NwASC is higher than expected.
This may be due to the amount of high saline water included in the calculations.

4.3 Temperature and Salinity

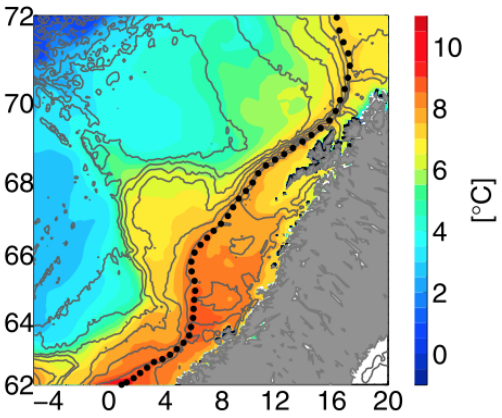

FIGURE 4.4: *Winter mean surface temperature (Isachsen, Koszalka, and LaCasce, 2012).*

The surface temperature distribution found in the MIKE model is relatively identical to the distribution found by Isachsen, Koszalka, and LaCasce (2012), figure 4.4.
The tongue of warm water transported by the current spreads out over the continental slope as it travels north along the coast with a maximum winter temperature of 10° C.

The characteristic wedged shape high salinity is shown not to be very seasonal dependent.

The width of the wedge in the Svinøy section is approximately 170 km. This is close to the width measured by the hydrographic stations of 200 km (Orvik, Skagseth, and Mork, 2001).

Vertically the saline water for the MIKE model reaches a mean depth of 1000 m which is approximately twice the depth of the measured saline depth at Svinøy of 450 m (Skagseth and Orvik, 2002).
This could account for the large transport through the Svinøy section.

Mork and Blindheim (2000) found that the inter-annual variation of temperature, salinity and transport in the Svinøy section primarily are controlled by large scale variable pressure system like the North Atlantic Oscillation index.

At the Lofoten section the high salinity and temperature is concentrated around the continental slope. In the beginning of the model run the salinity is widely spread out but diminishes fast.

Köhl (2007) found variations in both temperature and salinity in the LB near the center as indications of the quasi-permanent vortex. None of these variations can be found in the MIKE model.

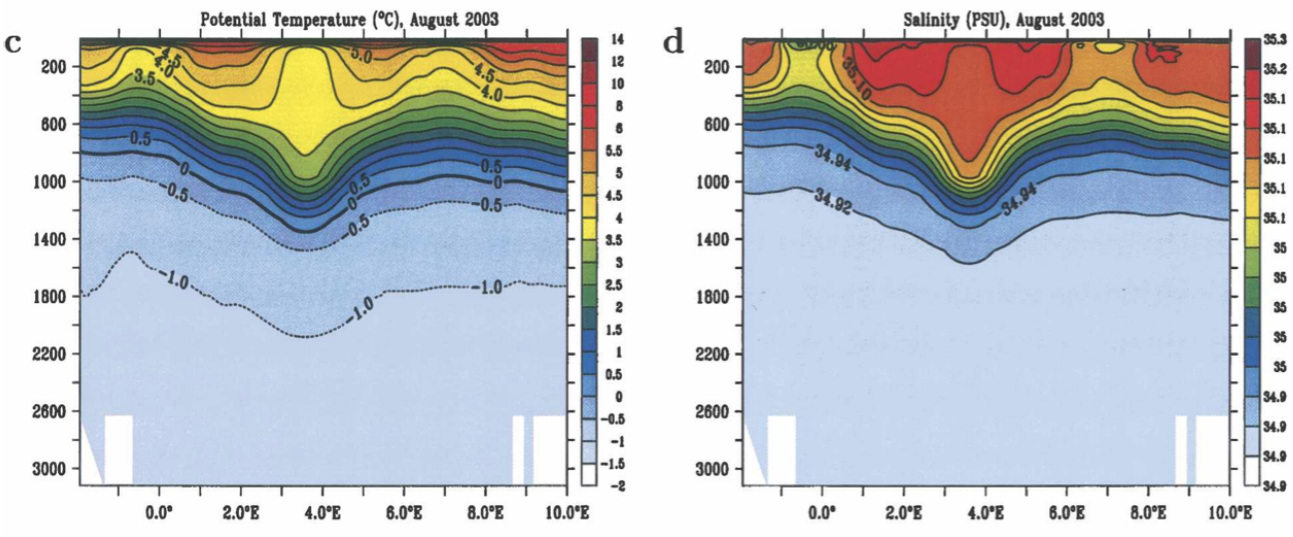

FIGURE 4.5: *Temperature* [$°C$] *and Salinity* [*psu*] *at LB (Köhl, 2007).*

4.4 Eddies

The formation of eddies and the strength of the current velocity are directly linked (Orvik and Skagseth, 2005; Skagseth, 2004). With the mean velocity of NwASC being slightly lower than expected and the NwAFC unaccounted for, the eddies created between the two currents are not to be seen.

Hansen, Kvaleberg, and Samuelsen (2010) found that the eddies and meanders in the area between NCC and NwASC are related to the smooth inshore topographic slope and the steep offshore drop. The eddies in this region exist but are sparsely spread.

Volkov, Kubryakov, and Lumpkin (2015) conducted three high-resolution experiments with varying grid spacing, 18 km, 9 km and 4 km. They found that the

vortex at LB did not form in the 18 km experiment and got the most realistic vortex simulation in the 4 km experiment compared to observation. This is because the grid spacing is greater than the Rossby radius of deformation in the LB.
A less coarse resolution could show an improved result for eddies.
The area between NwASC and the expected NwAFC at the Svinøy section holds a resolution of approximately 8 km and for the LB the resolution is up approximately 13 km. The resolution used by Johannessen et al. (2005) was $2 - 4$ km, but this would require a larger computer processors.

4.4.1 Eddy heat flux

The highest mean eddy heat flux produced by the data is around the area of Svinøy.

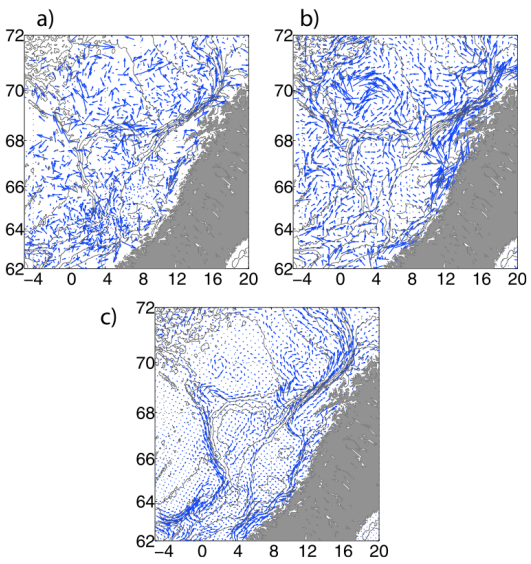

FIGURE 4.6: *eddy heat fluxes from a) drifters, b) satellite and c) model (Isachsen, Koszalka, and LaCasce, 2012).*

Compared to the results found by (Isachsen, Koszalka, and LaCasce, 2012), figure 4.6, there are some conformity in form of the location of eddy heat flux and areas of intensification.

The diffuseness of the heat flux at Svinøy shows most resemblance with the heat flux created with drifter data, whereas the satellite- and modelled heat flux are more aligned with the topography.

All of the figures in 4.6 shows a large heat flux at Lofoten which is not well represented in the MIKE model.

Figure 4.6 illustrates the heat flux for the autumn/winter period, where the direction of the flux is north-east following the continental slope. This is similar to the modelled result. Evidence of southward flux in spring/summer from measurement are yet to be found.

A longer model run could have an effect on the mean direction of the heat flux. More data from several years could prove if there is a seasonal tendency for a southward heat flux during spring and summer.

Jayne and Marotzke (2002) found that the majority of eddy heat flux is confined to the upper 1000 m of the ocean. For the MIKE model the heat flux does not enter water below 300 m and is decline substantially with the depth.

4.4.2 Eddy kinetic energy

The distribution of EKE both for the annual mean and the seasonal mean is very comparable with the EKE found by Andersson et al. (2011) and Koszalka et al. (2011) as seen in figure 4.7.

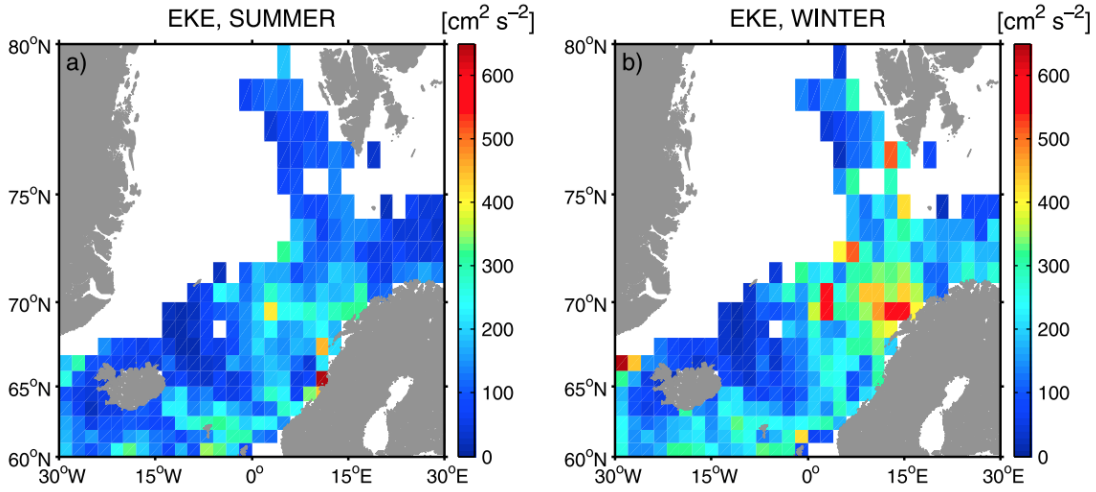

FIGURE 4.7: *Eddy kinetic energy computered from drogued drifter observation (Andersson et al., 2011).*

The area with the highest EKE is located near Lofoten, though a smaller area is found at Svinøy. The magnitude of the EKE is also quite alike.

Figure 4.7 shows the seasonal variation where there is an increase in the EKE during autumn/winter which is in agreement with the result from the MIKE model. Poulain, Warn-Varnes, and Niiler (1996) found that the EKE is greatest in regions with strong current, which is also evident in the results.

As for the current velocity the EKE is also connection to the wind forcing (Hansen, Kvaleberg, and Samuelsen, 2010).

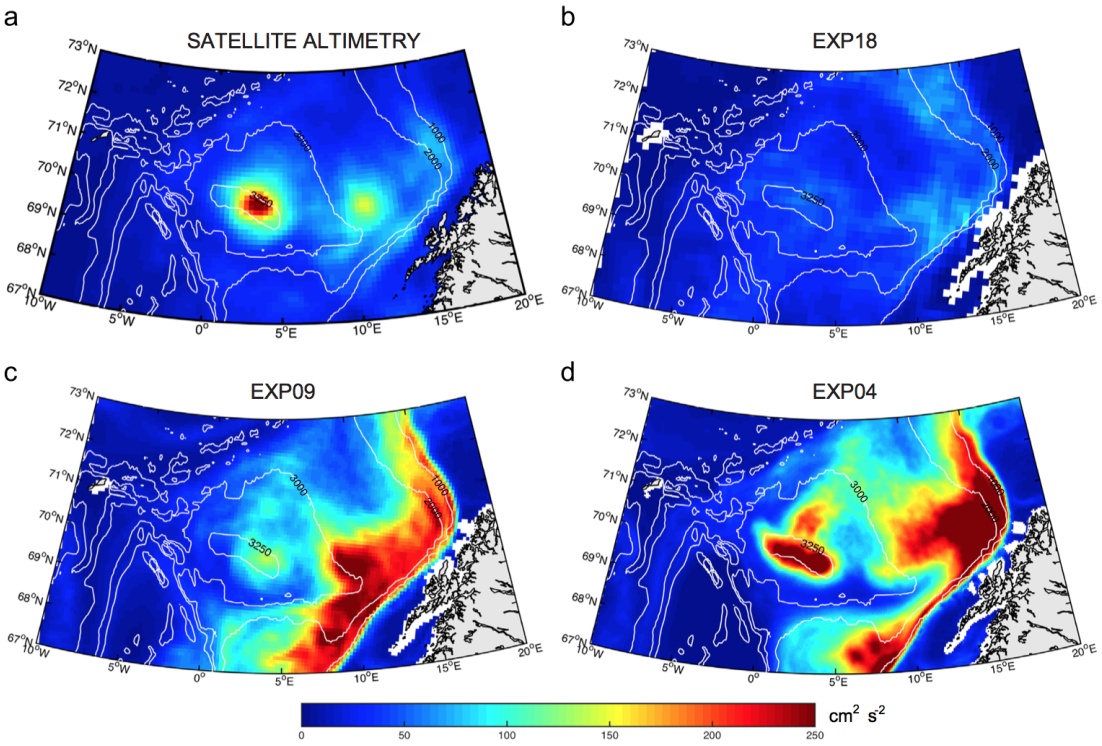

FIGURE 4.8: *Eddy kinetic energy estimated from satellite and model (Volkov, Kubryakov, and Lumpkin, 2015).*

Poulain, Warn-Varnes, and Niiler (1996) and Volkov, Kubryakov, and Lumpkin (2015) found a large EKE appearing in the LB with energies of 250 cm^2/s^2 as an indication of the quasi-permanent vortex, figure 4.8.
This EKE increase is not present in the MIKE model and there is no confirmation of the existence of the quasi-permanent vortex.

4.5 Validation

The model validations made by Rugbjerg (2014) have all been made in the proximity to the shore and areas with shallow water, figure 4.9.

The data comparison shows a satisfying result in these areas.

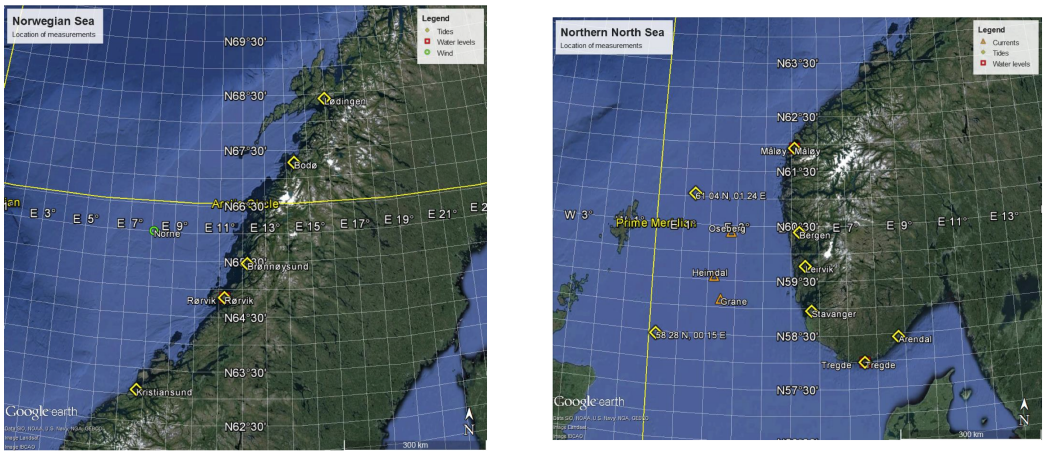

(A) *Mid Norway* (B) *South Norway*

FIGURE 4.9: *Location of the stations where comparisons between measurements and model have been made (Rugbjerg, 2014).*

For this thesis the same pattern occurs. The data near the continental shelf shows results that are quite similar to in-situ measurements in regards to salinity, temperature, current velocity and current path.
For the deeper ocean, the model does not give any useful results.

Chapter 5

Conclussion

5.1 Conclussion

This thesis has shown that the MIKE powered by DHI model covering the Norwegian Sea is able to describe the circulation of the Norwegian currents in the proximity of the coast and the continental slope.

The MIKE model showed a great ability in constructing the NwASC.
The topographically steered path was accurate, and the mean current velocity was close to the expected 0.3 $\mathrm{m\,s^{-1}}$ in certain areas.
The seasonal variation of the current was as expected, with a stronger current in the autumn and winter due to an intensified wind field.

The display of the NCC lacked a little. The current path was not clearly visual along the coast, and the velocity was in the low range, which made it difficult to distinguishes the NCC from the NwASC in certain areas.

The MIKE model could not produce the third current, NwAFC. In general there were no useful results for the deeper part of the Norwegian Sea.

The representation of the different water masses was good in the model. The warm and saline water characterizing the Atlantic Water was located over the slope along the coast as foreseen, making it easy to identify the NwASC.

The transport of warm, saline Atlantic Water was calculated based on the velocities of NwASC and prove to be too high for the single current, but with the assumption of a combined NwASC and NwAFC the transport was in the range of the expected.

The models representation of the eddy activity prove to be very good in the area over the continental shelf. There were no indications of the quasi-permanent vortex in the Lofoten basin, which is a the major heat reservoir in the Norwegian Sea and plays a key role in the heat flux.

In general the MIKE model has proven to be able to represent the features of the Norwegian Sea quite well in areas with water depth over 1000 m.

5.2 Further perspective

The MIKE model does not portray the NwAFS in the Norwegian Sea or the high eddy activity in the Lofoten Basin.
In order to use the model for these deeper regions in the Norwegian Sea, a new inflow of Atlantic Water should be added and the bathymetry of the model for the deeper water should be more refined.
A longer model run could also prove beneficial for the calculations of the eddy heat flux.

Bibliography

Amundsen, Bård and Else Lie (2011). *The Chaotic current that warms Norway.* URL: http://www.forskningsradet.no/prognett-norklima/Nyheter/The_chaotic_current_that_warms_Norway.

Andersson, M. et al. (2011). "Variability of the Norwegian Atlantic Current and associated eddy field from surface drifters." In: *Journal of geophysical research* 116.

Blindheim, Johan (1990). "Artic Intermediate water in the Norwegian Sea". In: *Deep Sea Research* 37, pp. 1475–1489.

Cheng, Y. and O. B. Andersen (2010). *Improvement of global ocean tide models in shallow water regions.*

DHI, MIKE by (2014). "MIKE 21 MIKE 3 flow model, Hydrodynamic and transport module, Scientific Documentation". In:

Grotefendt, Kerstin et al. (1998). "Is the Arctic Ocean warming?" In: *Journal of geophysical research* 103.C12, pp. 27679–27687.

Hansen, C., E. Kvaleberg, and A. Samuelsen (2010). "Anticyclonic eddies in the Norwegian Sea; their generation,evolution and impact on primary production." In: *Deep-Sea Research 1* 57, pp. 1079–1091.

Helland-Hansen, Bjørn and Fridtjof Nansen (1909). "The Norwegian Sea: Its physical oceanography based upon the Norwegian researches 1900-1904". In: *Report on Norwegian Fishery and Marine-investigations* 11.2, pp. 1–359.

Ikeda, M. et al. (1988). "A process study of mesoscale meander and eddies in the Norwegian Coastal Current". In: *Journal of physical oceanography* 19.

Isachsen, P. E., I. Koszalka, and J. H. LaCasce (2012). "Observed and modeled surface eddy heat fluxes in the eastern Nordic seas". In: *Journal of geophysical research* 117.

Isachsen, P. E. et al. (2003). "Wind-driven variability of the large-scale recirculating flow in the Nordic Seas and Arctic Ocean." In: *Journal of physical oceanography* 33, pp. 2534–2550.

James, I. D. (1991). "A primitive equation model simulation of eddies in the Norwegian Coastal Current". In: *Notes and correspondence*, pp. 893–902.

Jayne, Steven R. and Jochem Marotzke (2002). "The Oceanic Eddy Heat Transport." In: *Journal of physical oceanography* 32, pp. 3328–3345.

Johannessen, J. A. et al. (1989). “Three-Dimensional structure of mesoscale eddies in the Norwegian Coastal Current”. In: *Journal of physical oceanography* 19.

Johannessen, J. A. et al. (2005). “On radar imaging of current features: 2. Mesoscale eddy and current front detection.” In: *Journal of Geophysic research* 110.

Knauss, John A. (1997). *Introduction to physical oceanography.*

Koszalka, I. et al. (2011). “Surface circulation in the Nordic Seas from clustered drifters.” In: *Deep-sea research 1* 58, pp. 468–485.

Köhl, Armin (2007). “Generation and stability of a Quasi-Permanent vortex in the Lofoten Basin”. In: *Journal of physical oceanography* 37, pp. 2637–2651.

Ljøen, Rikard and Odd Nakken (1969). “On the hydrography of the shelf off Møre and Helgeland”. In: *FiskDiv. Skr. Ser. HavUnders* 15, pp. 285–294.

Mork, K. A. and Ø. Skagseth (2010). “A quantitative description of the Norwegian Atlantic Current by combining altimetry and hydrography.” In: *Ocean Science* 6, pp. 901–911.

Mork, Kjell Arne and Johan Blindheim (2000). “Variations in the Atlantic inflow to the Nordic Seas 1955-1996”. In: *Deep-Sea research* 1, pp. 1035–1057.

Mork, M. (1981). “Circulation phenomena and frontal dynamics of the Norwegian coastal current”. In: *Mathematical and physical Sciences* 302, pp. 123–135.

Mysak, Lawrence A. and Friedrich Schott (1977). “Evidence for baroclinic instability of the Norwegian current”. In: *Journal of geophysical research* 82.15, pp. 2087–2095.

Oey, Lie-Yauw and Ping Chen (1992). “A nested-grid ocean model: with application to the simulation of meanders and eddies in the Norwegian Coastal Current”. In: *Journal of geophysical research* 97.C12, pp. 20063–20086.

Orvik, Kjell Arild (2004). “The deepening of the Atlantic water in the Lofoten Basin of the Norwegian Sea, demonstrated by using an active reduced gravity model”. In: *Geophysical Research Letters* 31.

Orvik, Kjell Arild and Peter Niiler (2002). “Major pathways of Atlantic water in the northern North Atlantic and Nordic Seas toward Arctic”. In: *Geophysical research letters* 29.

Orvik, Kjell Arild and Øystein Skagseth (2005). “Heat flux variations in the eastern Norwegian Atlandic Current towards the Arctic from moored instruments, 1995-2005”. In: *Geophysical Research Letters* 32.

Orvik, Kjell Arild, Øystein Skagseth, and Martin Mork (2001). “Atlantic inflow to the Nordic Seas: current structure and volume fluxes from moored current meters, VM-ADCP and SeaSoar-CTD observations, 1995-1999”. In: *Deep-Sea research* 1, pp. 937–957.

Pedersen, O. P. et al. (2005). "Eddy formation on the coast of North Norway - evidence by synoptic sampling". In: *Journal of Marine Science* 62, pp. 615–628.

Poulain, P. M., A. Warn-Varnes, and P. P. Niiler (1996). "Near-surface circulation of the Nordic seas as measured by Lagrangian drifters." In: *Journal of geophysical research* 101.C8, pp. 18237–18258.

Raj, Roshin Pappukutty (2013). *The circulation of the Norwegian Sea - An investigation from space and ocean.*

Rugbjerg, Morten (2014). "Northern North Sea, Norwegian Sea and Barents Sea 3D Hydrodynamic Model". In: *DHI Internal Documentation.*

Røed, Lars Petter and Ingerid Fossum (2004). "Mean and eddy motion in the Skagerak/northern North Sea: insight from a numerical model." In: *Ocean Dynamics* 54, pp. 197–220.

Skagseth, Øystein (2004). "Monthly to annual variability of the Norwegian Atlantic slope current: connetion between the northern North Atlantic and the Norwegian Sea". In: *Deep-Sea research* 1, pp. 349–366.

Skagseth, Øystein and Kjell Arild Orvik (2002). "Identifying fluctuations in the Norwegian Atlantic slope current by means of empirical orthogonal functions". In: *Continental shelf research* 22, pp. 547–563.

Sætre, R. and R. Ljøen (1972). "The Norwegian coastal current". In: *Port and Ocean engineering under Arctic conditions*, pp. 514–535.

UNESCO (1981). "The practical salinity scale 1978 and the international equation of state of seawater 1980." In: *UNESCO technical papers in marine science* 33.

Volkov, Denis L., Arseny A. Kubryakov, and Rick Lumpkin (2015). "Formation and variability of the Lofoten basin vortex in a high-resolution ocean model." In: *Deep-Sea Research 1* 105, pp. 142–157.